JOURNAL OF GEOPHYSICAL RESEARCH, VOL. 91, NO. B1, PAGES 599-631, JANUARY 10, 1986

PERIDOTITES FROM THE ISLAND OF ZABARGAD (ST. JOHN), RED SEA: PETROLOGY AND GEOCHEMISTRY

Enrico Bonatti

Lamont-Doherty Geological Observatory of Columbia University, Palisades, New York

Giulio Ottonello

Istituto di Geocronologia e Geochimica Isotopica, Consiglio Nazionale delle Ricerche, Pisa, Italy

Paul R. Hamlyn

Department of Geology, University of Melbourne, Australia

Abstract. Exceptionally fresh peridotite bodies outcrop on Zabargad Island, an uplifted fragment of sub-Red Sea lithosphere. The peridotites are associated with basaltic dikes and are in tectonic contact with a metamorphic unit and with post-Mesozoic sedimentary units. The peridotites can be divided into three main groups: (1) protogranular spinel lherzolites (sp-lherzolites), with average modal composition ol 65%, opx 16%, cpx 16%, spinel 3% (2) amphibole peridotites (amph-peridotites), containing >2% magnesio-hornblende (3) plagioclase peridotites (pl-peridotites), containing >2% Ca-plagioclase. Minor outcrops of dunite and wherlite were also observed. The pl-peridotites and amph-peridotites, which are found in localized zones or bands within the sp-lherzolite, show textures ranging from porphyroclastic to cataclastic, indicating varying degrees of tectonic deformation. Olivine and opx have a rather constant composition in the three groups, Fo ranging between 87.3% and 90.5% and En between 88% and 89%, respectively. Clinopyroxene is chromian diopside but contains less Na in the pl-peridotites than in the sp-lherzolites. Both opx and cpx are moderately Al and Cr-rich, as is typical of mantle-equilibrated pyroxenes. Spinel has a very low Cr/Al ratio in the sp-lherzolites, lower than in the pl- and amph-peridotites. Plagioclase in the pl-peridotites ranges between An 80% and 93%, while traces of it rimming spinel in some of the sp-lherzolites are more sodic. The amph- peridotites contain up to 28% magnesio-hornblende and, in some cases, traces of phlogopite and apatite; opx, cpx, and spinel are scarce. The major element composition of the Zabargad sp-lherzolites, their slight light rare earth element (LREE)-depleted pattern, transition elements Sc, Ti, Cr, Mn, Fe, Co, and Ni data, together with modal and mineral chemistry data, are all consistent with the sp-lherzolites having last equilibrated in the sp-lherzolite stability field (>9 kbar, >30 km deep) and representing essentially undepleted parental mantle material, though some samples might have undergone minor partial melting. The pl-peridotites may represent localized incorporation of a melt component by the ascending lherzolite body. The amph-peridotites are enriched in K, LREE, and occasionally in P relative to sp-lherzolites; they were probably formed by localized contamination with H20-rich metasomatic fluids injected through the lherzolite body during its ascent. The Zabargad peridotites were probably emplaced from the upper mantle into the crust during the development of the Red Sea rift, i.e., in post-Mesozoic time. They show affinity with some mantle- derived oceanic ultramafics, particularly with St. Paul Rocks in the Atlantic. They could be considered a sample of oceanic mantle before extraction of the basaltic oceanic crust.

Paper number 5B5686.
0148-0227/86/005B-5686$05.00

Introduction

The island of Zabargad (or St. John) in the central Red Sea exposes exceptionally fresh mantle-derived peridotites. It is located at 23°37'N, 36°12'E (Figure 1) about 50 km west of the axis of the Red Sea, in an area of great geotectonic interest, i.e., a zone transitional between oceanic and continental lithosphere within a young rift formed by the breakup of a continent. The island is probably a tectonically uplifted fragment of sub-Red Sea lithosphere [Bonatti et al., 1981, 1983]. Even though the island has been known since antiquity as a source of gem-quality olivine crystals, and though for over 50 years ultramafic rocks have been known to outcrop there [Moon 1923], the Zabargad peridotites have never, to our knowledge, been the object of a modern study. During two field trips in 1979 and 1980, as part of a broad study of the geology of the central Red Sea between 22°N and 25°N, we carried out field work on the island, which included a thorough sampling of the peridotites and of the other exposed lithologic units. In this paper we report a first general overview of the petrology and geochemistry of the Zabargad peridotites, which follows a preliminary note on the same subject [Bonatti et al., 1981] and will be followed by more detailed studies.

Zabargad Peridotites: Field Observations

The geology of Zabargad, first described by Moon [1923], has been discussed in detail recently by Bonatti et al. [1983]. Briefly, the island exposes the following lithologic units (Figure 1): (1) peridotites, which outcrop in three main bodies and constitute the main lithological unit exposed on the island, (2) metamorphic unit, possibly equivalent to a Pan-African Precambrian unit exposed in the Eastern Desert region of Egypt and Sudan, (3) basaltic-doleritic dikes and shallow intrusions, found within the peridotitic and metamorphic units, (4) limestone-sandstone-black shale formation (Zabargad Formation), probably of late Cretaceous or Paleocene age, (5) evaporites, probably of Miocene age, (6) older coral reefs, uplifted up to 60 m above present sea level, of late Pliocene-early Pleistocene age, (7) younger and Recent reefs, and (8) Recent beach and detrital deposits.

Peridotites outcrop at Zabargad in three main bodies which

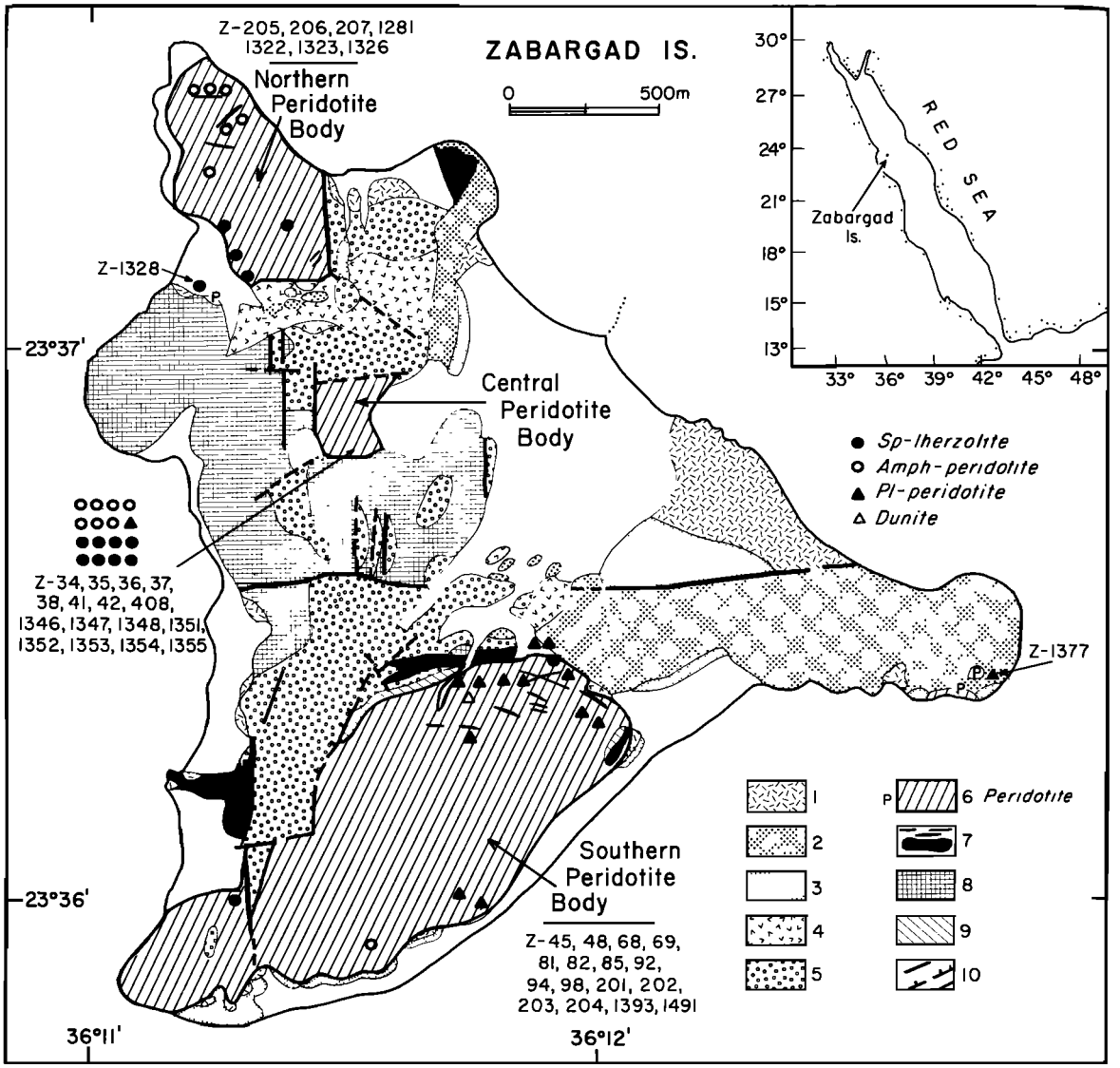

Fig. 1. Simplified geological map of the island of Zabargad [from Bonatti et al., 1983]. 1, young reef limestone (late Pleistocene); 2, old reef limestone (early Pleistocene); 3, breccia and conglomerate; 4, Evaporite Unit (Miocene); 5, Zabargad Sedimentary Formation (Cretaceous- Paleocene); 6, Peridotite Unit (the Southern, Central, and Northern Peridotite Bodies are indicated; symbols indicate samples of different peridotite facies; locations of samples considered in this paper are shown; 7, basalt and dolerite dikes and shallow intrusions; 8, Metamorphic Unit; 9, gabbros; 10, principal faults.

we call the Southern, Central, and Northern Peridotite Bodies (Figure 1). The Southern Peridotite Body makes up the bulk of the highest relief of the island, rising along its SE shore up to 265 m above sea level ("Main Peridotite Hill" of Moon [1923]). Contacts with other units, particularly the metamorphic unit, appear to be tectonic [Bonatti et al., 1983].

A mild foliation was observed in discrete zones within some exposed sections of the peridotite. The prevalent orientation of the foliation is roughly NW-SE [Piccardo and Ottonello, in preparation], that is, parallel to the general orientation of the Red Sea. The ultramafic bodies are dissected by systems of fractures. The prevalent systems strike close to E-W in the Southern Peridotite Body, parallel to a major fault separating this body from other units on its northern side (Figure 1), and close to N-S in the other peridotite bodies, parallel to a fracture zone which intersects the Red Sea at the latitude of Zabargad [Bonatti et al., 1984]. Other structural directions are also present on the island but are less frequent. Basaltic-doleritic dikes ranging in thickness from several meters to centimeters frequently cut the ultramafic rocks striking preferentially along the aforementioned structural directions. Pyroxenite bands and veins cutting through the peridotites were also observed.

The peridotites appear generally very fresh, displaying the classic olive green color in freshly cut sections, except for a reddish-yellow patina of surficial weathering which extends also within fractures. An exception is the fault zone at the NE side of the Southern Peridotite Body (Figure 1), where the peridotite is strongly altered into powdery yellow serpentinitic material and where Ni-(garnierite) and Ca-rich (with cancrinite and scapolite) mineralizations are located [El Shazly and Saleeb, 1972]. This is also the zone where large gem-quality olivine crystals were mined in the past. These olivines are generally in the form of radial crystal aggregates embedded in a matrix of serpentinitic material.

Samples were collected from each of the three main

TABLE 1. Average Modal Composition of Zabargad sp-Lherzolites, amph-Peridotites, pl-Peridotites, and pl-amph-Peridotites

	ol	opx	cpx	sp	pl	amph
sp-lherzolite (Z-34-37-42-48-1328-1352)	65	16	16	3	-	-
pl-peridotite (Z41-68-81-94-98)	62	11	9	2	16	-
amph-peridotite (Z-206-1348-1354)	68	5	1	2	-	21
pl-amph-peridotite (Z-45-203-207-1481)	65	8	5	2	12	6

Values are in percent. Data were obtained by point counting in thin section under the microscope. A minimum of 600 points were counted in each sample, spaced 0.5 μm apart. Grain size of the rocks ranges from 0.1 to 1 cm.

peridotite bodies (Figure 1). A particularly closely spaced set of samples was obtained from a section roughly 20 m thick, exposed by a small erosional wadji in the Central Peridotite Body.

Petrography of the Peridotites

Textures

The exceptional freshness of the samples is confirmed by the absence of serpentine minerals in most of them. A number of samples appear relatively undeformed under the microscope (Figure 2), displaying protogranular [Mercier and Nicolas, 1975], or coarse-mosaic [Harte, 1977] textures. In these samples, relatively large (several millimeters) olivine and opx crystals coexist with slightly smaller (<1 mm) cpx and spinels. Olivine crystals commonly display undulatory extinction, kink bands, and systems of fractures with no apparent preferred orientation. Occasionally, large crystals have recrystallized into mosaics of smaller crystals. Spinel tends to be found toward the margins of, or within, larger enstatite crystals or between opx and cpx boundaries. No foliation is observed in these rocks.

The protogranular lherzolites grade into rocks showing a range of textures from porphyroclastic to cataclastic, as defined by Mercier and Nicolas [1975] and Pike and Schwarzman [1977]. Larger olivine and enstatite porphyroclasts, generally elongated and strained and frequently showing kinking and undulatory extinction, are set in a matrix of smaller (≈1 mm) scattered crystals, among which are spinels often showing foliation with the same orientation of the porphyroclasts (Figure 2). In some samples the matrix consists of strained and broken, comminuted small crystals (cataclastic texture) (Figure 2). Strings of broken grains, in addition to orientation of porphyroclasts, give foliation to the rock. Cataclastic textures are rare, while porphyroclastic textures are relatively common.

Some relationship appears to exist between modal composition and texture in these rocks. Protogranular textures are found exclusively in sp-lherzolites with <2% modal amphibole and/or plagioclase. Samples containing significant amphibole and/or plagioclase tend to be tectonically deformed to various degrees, showing porphyroclastic or cataclastic textures.

The degree of deformation of the Zabargad peridotites can vary locally within very short distances (a meter as an order of magnitude). A closely sampled section in the Central Peridotite Body, about 20 m thick, yielded undeformed protogranular lherzolites but also levels with various degrees of tectonic deformation and foliation and with textures ranging from porphyroclastic to cataclastic.

Modal Composition

On the basis of modal composition, estimated qualitively by X ray diffractometry on powdered samples and semiquantitatively by point counting under the microscope (Table 1), the Zabargad peridotites can be divided into three main groups (Figure 3):

Spinel lherzolites, characterized by the assemblage olivine-enstatite-diopside-spinel. Plagioclase was found in trace amounts (<1%) in some samples as aggregates <5 μm thick, rimming spinel crystals (Figure 4). A few of these rocks contain trace amounts of a brown amphibole, in small (<5 μm) crystals generally associated with either cpx or spinel and/or phlogopite. The large majority of these sp-lherzolites display protogranular textures (Figure 2).

Plagioclase peridotites, containing plagioclase as a significant (> 2%) component. As plagioclase becomes more abundant, the width of the plagioclase selvages aroung spinel broadens. Simultaneously, spinel becomes more intergranular and wispy in appearance. In the rocks highest in plagioclase content the spinel crystals are surrounded by a broad (≈0.5-1 mm) zone of equigranular plagioclase. A similar spinel-plagioclase association has been described from the Lanzo [Boudier, 1978] and the Ronda peridotite massifs [Dickey,1970]. Some of the plagioclase-rich samples show plagioclase-rich veins forming a braided network around elongated lherzolite lenses, resulting in foliation of the rock.

Amphibole-peridotites, containing amphibole as a significant (>2%) component. Where amphibole is abundant, as for instance in sample Z-206, it is as pervasive pale green pleochroic laths replacing pyroxene. Brown Al-Cr-spinel crystals, as found in the sp-lherzolites, are absent in this sample, which contains instead small opaque grains of chromite and magnetite scattered throughout the rock, particularly within and around amphibole grains. Interstitial apatite is present in this rock. Traces of phlogopite and of Fe-Ni sulfide are present in some of the amph-peridotites.

Rocks intermediate in modal composition relative to the three groups are present, for instance, some pl-amph-peridotites. In addition to the three major rock groups, some minor outcrops of dunite and wehrlite were also sampled.

We note that the modal composition of the Zabargad peridotites can change within short distances (of the order of 1 m). Thus the aforementioned closely sampled ≈20 m section in the Central Peridotite Body yielded protogranular sp-lherzolites as well as porphyroclastic and cataclastic pl-peridotites and amph-peridotites.

Mineral Chemistry

Mineral compositions were determined on polished sections with an automated, 3-spectrometer ARL-EMX SM electron

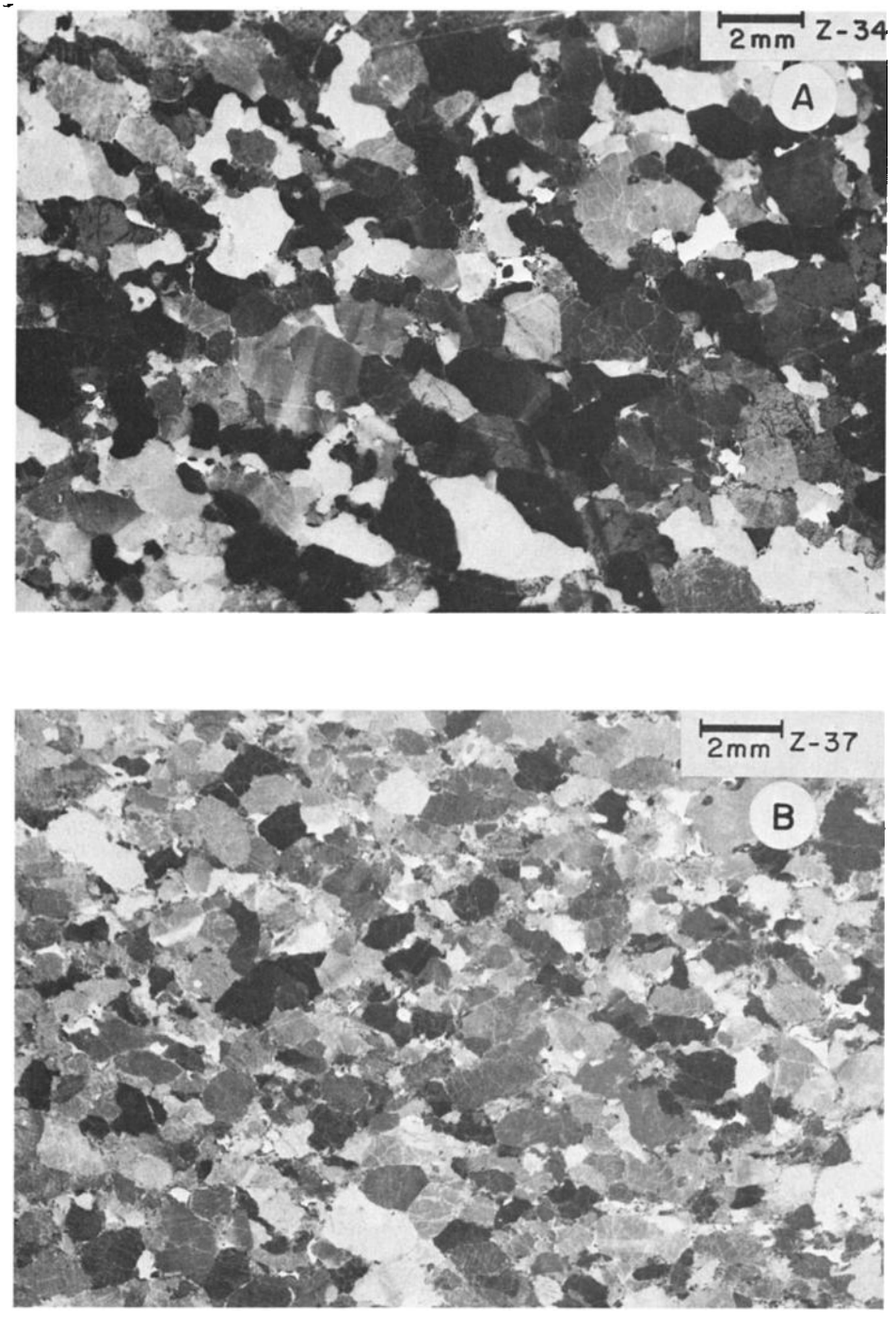

Fig. 2. Texture of Zabargad peridotite samples, illustrated by photographs of thin sections taken with polarized light. From Figure 2a to 2f, increasing degree of tectonic deformation, from protogranular to porphyroclastic and cataclastic.

microprobe. Data were reduced on-line using a modified Bence-Albee procedure, and reference to natural and synthetic mineral standards.

Olivine

Olivine is the major modal component of the various types of Zabargad peridotites (Table 1). The Fo content is relatively constant in the olivines from the three main peridotite groups (Table 2 and Figure 5) ranging from 87.3% to 90.5% Fo. This Fo content, as well as the NiO (3000-4000 ppm), CaO (0.03-0.14%), and MnO (0.11-0.17%) contents, are similar to those of olivines from tectonitic peridotites of mantle derivation recovered from the ocean basins [Prinz et al., 1976; Hamlyn and Bonatti, 1980; Arai and Fujii, 1979]. Olivines from pl-peridotites Z-35 and Z-69 have a slightly lower Fo and NiO content than those from the other Zabargad peridotites. Olivine from another pl-peridotite (Z-41), though rather low in Fo content, has normal NiO concentrations.

The large (centimeter size) gem-quality olivine crystals

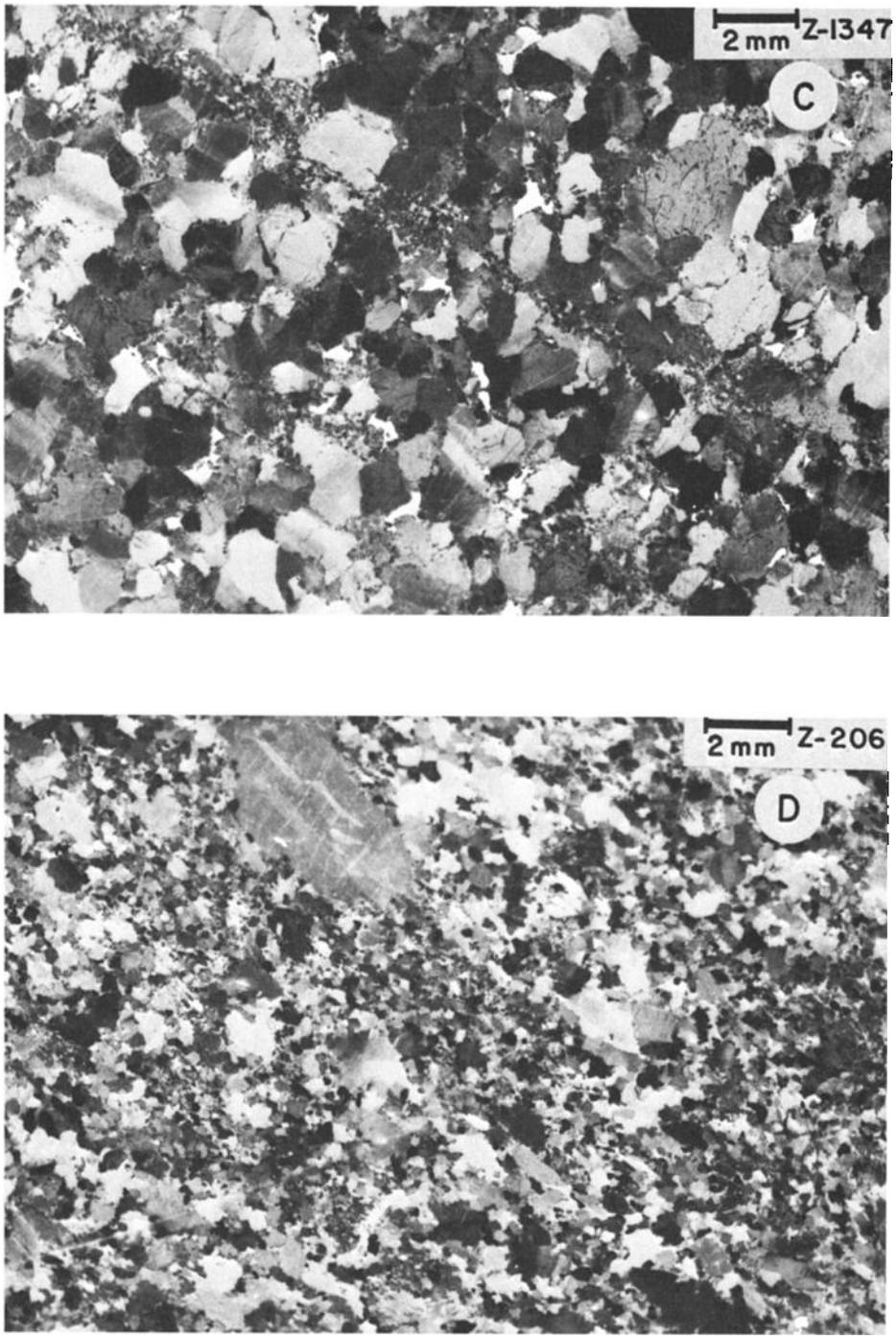

Fig. 2. (continued)

found within the altered zone on the northern side of the Southern Peridotite Body have a Fo content within the range of the Zabargad sp-peridotite olivines (Table 2), although their origin is different. They contain inclusions of talc, amphibole, chlorides, sulfates, carbonates, and phosphates, which are absent in the sp-lherzolite olivines [Clocchiatti et al., 1981]. The gem olivines probably crystallized as a result of reactions between a metasomatic, volatile-rich fluid and peridotite. These reactions took place at a temperature higher than the stability of serpentine (>500°C) but at a relatively low pressure.

Pyroxenes

Orthopyroxene and cpx compositions in the different peridotite groups (Tables 3 and 4) all cluster closely within the enstatite and diopside fields, respectively (Figure 6). Both the enstatites and the diopsides are moderately rich in Al and Cr, as is typical of mantle-equilibrated pyroxenes. The Al content of both opx and cpx falls toward the high range of pyroxene compositions in mantle-derived tectonitic peridotites from the ocean basins (Figures 7 and 8).

TiO_2 in opx from the sp-lherzolites ranges from 0.07 to

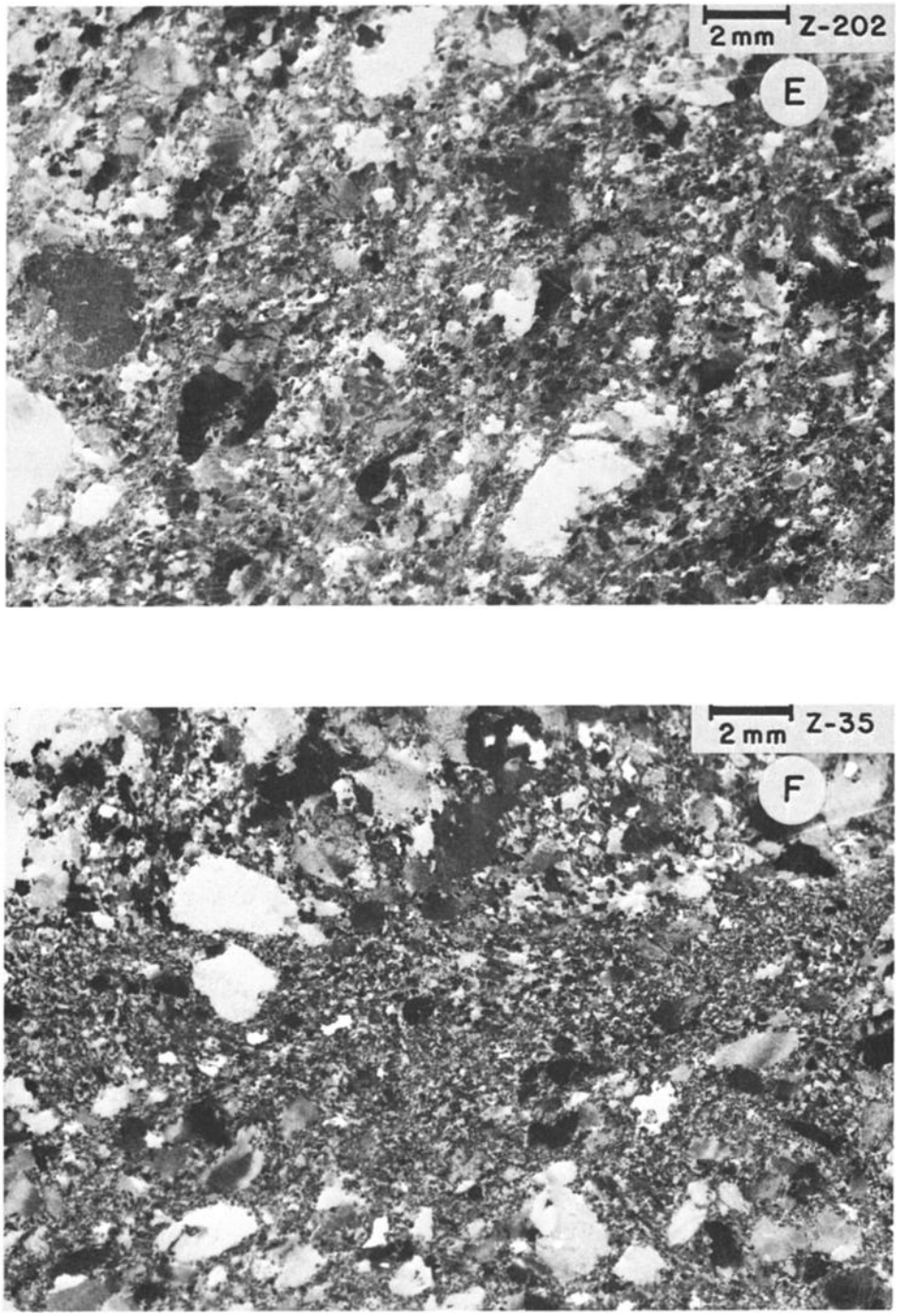

Fig. 2. (continued)

0.15%, i.e., within the range of opx from oceanic mantle-derived lherzolites. Orthopyroxene and cpx from the pl-peridotites tend to be higher in TiO_2 than those from sp-lherzolites (Figure 9). The Na content of the cpx in the sp-lherzolites is higher than in the pl-peridotites (Figure 9), while the Ca content has a broader range in the pl-peridotites than in the sp-lherzolite. Na and TiO_2 are higher in cpx of the Zabargad lherzolites than in those of mantle-derived oceanic peridotites [Bonatti and Hamlyn, 1981], exemplified by the Owen Fracture Zone lherzolites.

A lower Na content of cpx from pl-peridotite facies relative to sp-lherzolite facies within the same ultramafic body, as found at Zabargad, has been observed in other ultramafic complexes, for instance the Ronda massif [Kornprobst et al., 1981], and also in oceanic peridotites [Dick and Bullen, 1984]. This loss of Na in the cpx can be attributed to (1) transfer of Na from cpx to plagioclase during recrystallization-reequilibration from higher-P sp-lherzolite facies to lower-P pl-peridotite facies (2) extraction of Na from the solid during partial melting events, resulting in residual low-Na cpx [Kornprobst et al., 1981] and (3) extraction of Na from the cpx during reactions between a trapped melt fraction and the sp-lherzolite.

We estimated equilibration temperatures for some of the

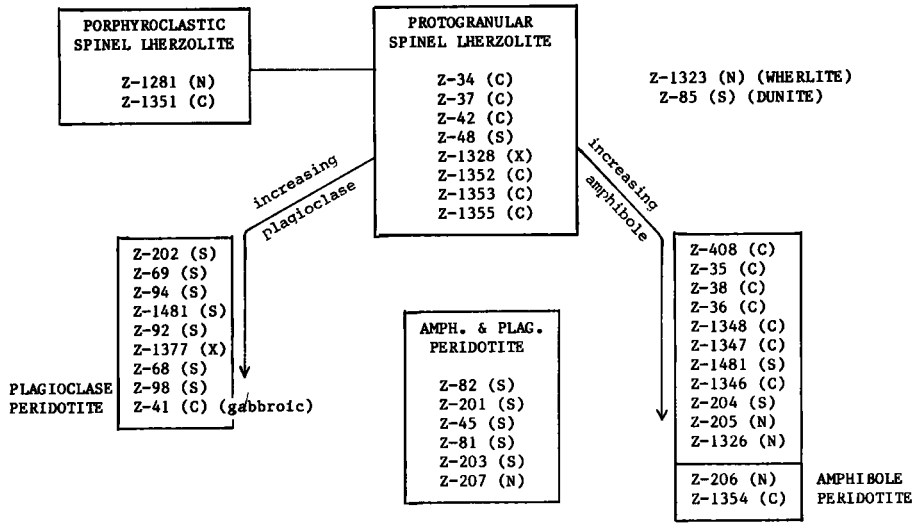

Fig. 3. Schematic classification of Zabargad ultramafic rock samples used in this study. Letters in parenthesis indicate location of the samples; N, Northern Peridotite Body; C, Central Peridotite Body; S, Southern Peridotite Body; X, isolated outcrops. (see Figure 1.)

sp-lherzolites and pl-peridotites using Wells' [1977] two-pyroxene geothermometry (Table 5). The calculated temperatures are similar in the two groups.

Spinel

The chemistry of spinels (Table 6) in the sp-lherzolite group is rather constant but is different from that of the other groups. The sp-lherzolites contain Al-rich, Cr-poor spinels, with Cr/(Cr+Al) ratios (Figure 10) lower than in spinels of mantle-derived oceanic peridotites, such as those from the Vema and Owen Fracture Zones [Bonatti and Hamlyn, 1981] and other Atlantic sites [Dick and Bullen, 1984; Michael and Bonatti, 1985]. The TiO_2 content of the Zabargad peridotite spinels is low (<0.5%), as in mantle-derived oceanic peridotites, but different from spinels of oceanic cumulus ultramafics [Bonatti and Hamlyn, 1981] and of oceanic basalts [Sigurdsson and Schilling, 1976].

The higher Cr/(Cr+Al) ratio of spinels from Zabargad pl-peridotites relative to sp-lherzolites could be related to subsolidus reequilibration of the ultramafic assemblage due to reduced pressure during ascent of the mantle body, through reactions of the type opx + cpx + Al-spinel = ol + pl + Cr-spinel. This kind of change in spinel chemistry with pressure of equilibration has been verified experimentally [Green et al., 1972], and has been suggested to explain

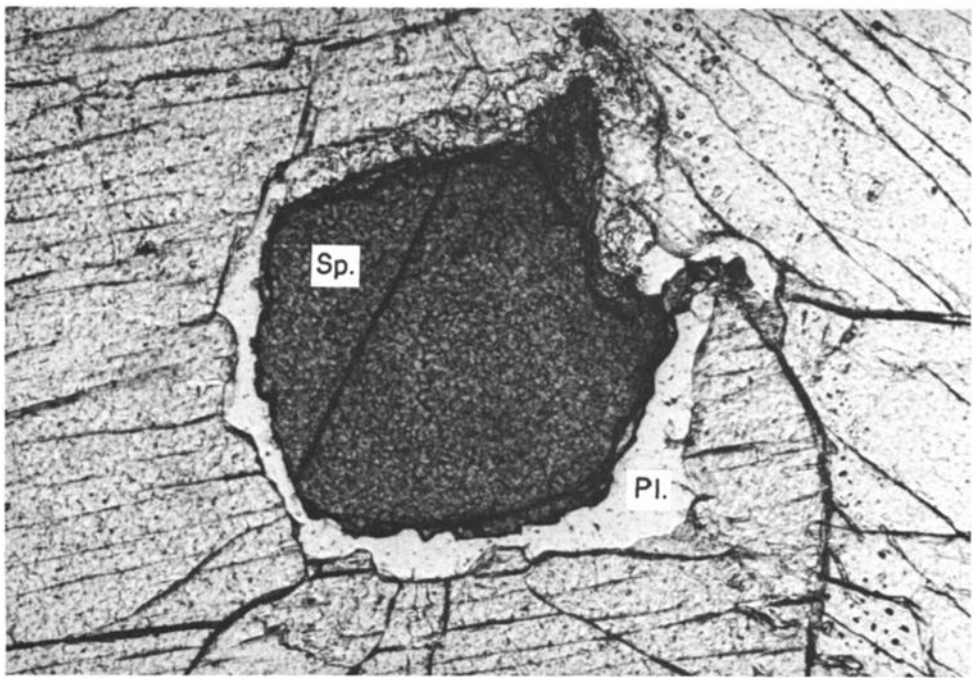

Fig. 4. Spinel crystal in Z-37 sp-lherzolite, showing a thin rim of plagioclase (An 55%) around spinel. Diameter of spinel crystal is about 30 μm.

TABLE 2. Electron Probe Chemical Analyses of Olivines From Zabargad Peridotites

	sp-Lherzolite			pl-Peridotite		
	Z-37	Z-34	Z-42	Z-98	Z-94	Z-69
SiO_2	39.59	39.50	40.90	40.90	40.80	40.50
TiO_2	0.00	0.00	0.00	0.03	0.03	0.00
Cr_2O_3	0.03	0.00	0.00	0.00	0.00	0.00
FeO	10.72	10.90	10.20	10.40	9.99	11.90
MnO	0.17	0.14	0.14	0.17	0.14	0.26
NiO	0.33	0.35	0.42	0.30	0.40	0.20
MgO	49.14	48.10	47.60	48.30	48.50	45.90
CaO	0.13	0.04	0.11	0.03	0.14	0.12
K_2O	0.06	0.09	0.05	0.07	0.01	0.05
Total	100.17	99.12	99.42	100.20	100.01	98.93
	Structural Formula Based on Four Oxygens					
Si	0.977	0.986	1.011	1.004	1.002	1.013
Ti	0.000	0.000	0.000	0.001	0.001	0.000
Cr	0.001	0.000	0.000	0.000	0.000	0.000
Fe^{2+}	0.221	0.227	0.211	0.213	0.205	0.249
Mn	0.004	0.003	0.003	0.004	0.003	0.006
Ni	0.007	0.007	0.008	0.006	0.008	0.004
Mg	1.808	1.789	1.753	1.767	1.775	1.711
Ca	0.003	0.001	0.003	0.001	0.004	0.003
K	0.002	0.003	0.002	0.002	0.000	0.002
Total	3.023	3.016	2.990	2.997	2.998	2.988
Fo	89.09	88.72	89.27	89.22	89.64	87.30
Fa	10.91	11.28	10.73	10.78	10.36	12.70

	amph-Peridotite		amph-pl-Peridotite	Gabbroic	Gem	
	Z-35	Z-206	Z-45	Z-41	Gem 1	Gem 2
SiO_2	39.70	40.20	40.45	40.00	40.77	41.52
TiO_2	0.02	0.00	0.00	0.03	0.00	0.00
Cr_2O_3	0.00	0.00	0.03	0.00	0.00	0.00
FeO	11.20	9.82	9.11	10.80	9.95	9.88
MnO	0.11	0.16	0.09	0.14	0.14	0.11
NiO	0.20	0.33	0.36	0.38	0.37	0.30
MgO	47.90	47.90	48.86	48.10	48.70	49.64
CaO	0.07	0.11	0.07	0.07	0.13	0.07
K_2O	0.03	0.05	0.05	0.02	0.06	0.05
Total	99.23	98.57	99.02	99.54	100.12	101.57
	Structural Formula Based on Four Oxygens					
Si	0.989	1.002	1.000	0.992	1.000	1.002
Ti	0.000	0.000	0.000	0.001	0.000	0.000
Cr	0.000	0.000	0.001	0.000	0.000	0.000
Fe^{2+}	0.233	0.205	0.188	0.224	0.204	0.199
Mn	0.002	0.003	0.002	0.003	0.003	0.002
Ni	0.004	0.007	0.007	0.008	0.007	0.006
Mg	1.779	1.779	1.800	1.778	1.781	1.786
Ca	0.002	0.003	0.002	0.002	0.003	-
K	0.001	0.002	0.002	0.001	0.002	0.002
Total	3.011	2.999	3.001	3.008	3.001	2.999
Fo	88.40	89.68	90.53	88.81	89.72	89.95
Fa	11.60	10.32	9.47	11.19	10.28	10.05

Gem, large gem-quality olivine crystals (see text).

TABLE 3. Electron Probe Chemical Analyses of Clinopyroxenes From Zabargad Peridotites

	sp-Lherzolite			amph-pl- Peridotite	pl-Peridotite		Gabbroic
	Z-37	Z-34	Z-42	Z-45	Z-94(s)	Z-98	Z-41
SiO_2	50.87	51.90	46.30	49.62	47.00	48.10	44.40
TiO_2	0.61	0.82	0.61	0.43	0.72	1.63	1.14
Al_2O_3	6.47	7.31	6.22	6.10	2.64	5.21	6.58
Cr_2O_3	0.68	0.75	0.80	1.05	0.79	0.91	0.29
FeO	2.62	3.02	2.71	2.71	2.45	2.89	3.36
MnO	0.08	0.01	0.07	0.08	0.11	0.13	0.05
NiO	0.01	0.03	0.04	0.06	0.04	0.01	0.07
MgO	15.13	14.80	15.60	15.32	16.60	15.50	15.10
CaO	21.79	19.30	21.20	22.54	23.20	22.50	22.90
Na_2O	1.23	2.20	1.41	0.59	0.58	0.52	0.44
K_2O	0.07	0.08	0.06	0.04	0.06	0.07	0.04
Total	99.56	100.22	100.22	98.54	100.59	99.56	99.77
	Structural Formula, Based on Six Oxygens						
Si	1.858	1.872	1.866	1.839	1.932	1.843	1.825
Ti	0.017	0.022	0.017	0.012	0.020	0.045	0.031
Al	0.278	0.311	0.266	0.266	0.113	0.225	0.284
Cr	0.020	0.021	0.023	0.031	0.023	0.026	0.008
Fe^{2+}	0.080	0.091	0.091	0.082	0.084	0.074	0.089
Mn	0.002	0.000	0.002	0.003	0.003	0.004	0.002
Ni	0.000	0.001	0.001	0.002	0.001	0.000	0.002
Mg	0.824	0.796	0.843	0.846	0.895	0.848	0.825
Ca	0.853	0.746	0.823	0.895	0.899	0.885	0.899
Na	0.087	0.154	0.099	0.042	0.041	0.036	0.031
K	0.003	0.004	0.003	0.002	0.003	0.003	0.002
Total	4.022	4.018	4.024	4.022	4.003	4.006	4.013
En	46.90	48.74	48.21	46.36	47.91	46.55	45.15
Fs	4.56	5.58	4.70	4.60	3.97	4.87	5.64
Wo	48.55	45.68	47.09	49.03	48.13	48.58	49.22

(s) = small grains. Broad beam (≈80μm) was used.

bimodal spinel chemistry in the Owen Fracture Zone mantle-derived peridotites [Hamlyn and Bonatti, 1980]. Alternatively, if the pl-peridotites were due to localized introduction of an exotic melt fraction into the ascending lherzolite body (see discussion above), reactions of the melt with Al-rich spinel may have produced Cr-rich spinel plus plagioclase.

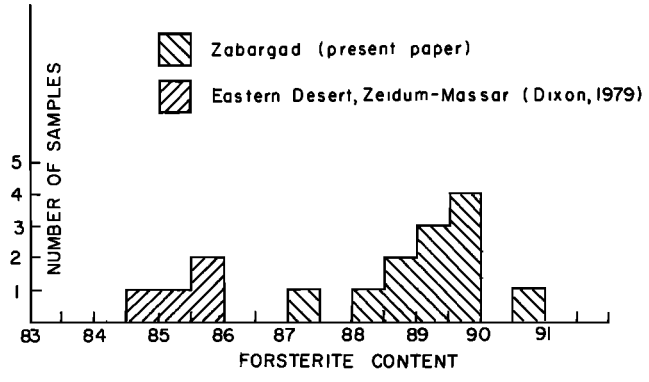

Fig. 5. Forsterite content of olivines from Zabargad peridotites, compared with those from the Zeidun-Massam ultramafic massif in the Eastern Desert region of Egypt, from Dixon [1979].

Amphiboles

The amphiboles contained in trace amounts in some of the protogranular sp-lherzolite (Z-37, for example) are compositionally different from those of amph-peridotites where amphiboles are a major constituent (Z-206, for example) and occur as larger crystals scattered throughout the rock (Table 7). The trace quantity amphiboles of some of the Zabargad sp-lherzolites are pargasitic, according to Leake's [1968] classification, while those of the amph-peridotites are magnesio-hornblende (Figure 11). The temperature of crystal-

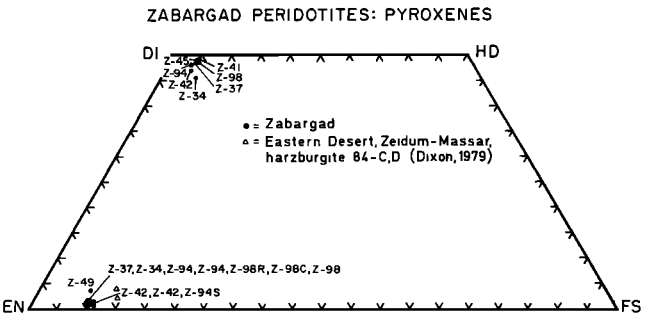

Fig. 6. Composition of pyroxenes of the Zabargad peridotites, plotted on a Poldervaart and Hess [1951] Di-Hd-En-Fs diagram and compared to pyroxenes from the Zeidun-Massam peridotite massif, from Dixon [1979].

TABLE 4. Electron Probe Chemical Analyses of Orthopyroxenes From Zabargad Peridotites

	sp-Lherzolite				amph-pl-Peridotite
	Z-37	Z-34	Z-42a	Z-42b	Z-45
SiO_2	54.03	54.20	56.00	57.30	54.45
TiO_2	0.15	0.14	0.10	0.07	0.10
Al_2O_3	3.97	3.86	3.50	2.89	3.89
Cr_2O_3	0.26	0.28	0.25	0.22	0.76
FeO	7.11	7.06	6.70	6.34	5.88
MnO	0.18	0.12	0.18	0.16	0.15
NiO	0.02	0.01	0.00	0.04	0.20
MgO	33.13	33.80	33.50	33.70	32.05
CaO	0.67	0.48	0.49	0.55	1.82
Na_2O	0.01	0.00	0.00	0.00	0.01
K_2O	0.05	0.07	0.08	0.10	0.06
Total	99.58	100.02	100.80	101.37	99.37
			Structural Formula		
Si	1.886	1.883	1.921	1.949	1.902
Ti	0.004	0.004	0.003	0.002	0.003
Al	0.163	0.158	0.142	0.116	0.160
Cr	0.007	0.008	0.007	0.006	0.021
Fe^{2+}	0.208	0.205	0.192	0.180	0.172
Mn	0.005	0.004	0.005	0.005	0.004
Ni	0.001	0.000	0.000	0.001	0.006
Mg	1.724	1.750	1.713	1.708	1.668
Ca	0.025	0.018	0.018	0.020	0.068
Na	0.001	0.000	0.000	0.000	0.001
K	0.002	0.003	0.004	0.004	0.003
Total	4.026	4.032	4.004	3.991	4.007
En	88.11	88.70	89.07	89.50	87.43
Fs	10.61	10.40	9.99	9.45	9.00
Wo	1.28	0.91	0.94	1.05	3.57

	pl-Peridotite					
	Z-94a	Z-94(s)	Z-94b	Z-98(r)	Z-98(c)	Z-98
SiO_2	53.90	55.40	56.10	55.50	55.10	54.80
TiO_2	0.20	0.17	0.20	0.66	0.42	0.43
Al_2O_3	4.04	1.50	2.65	2.13	2.63	3.68
Cr_2O_3	0.70	0.29	0.69	0.57	0.63	0.57
FeO	6.53	6.72	6.55	7.23	6.81	7.00
MnO	0.11	0.16	0.14	0.13	0.18	0.16
NiO	0.07	0.00	0.01	0.10	0.01	0.01
MgO	33.50	35.50	32.80	32.30	32.30	32.90
CaO	0.73	0.47	0.60	0.30	0.68	0.59
Na_2O	0.00	0.00	0.00	0.00	0.00	0.00
K_2O	0.03	0.03	0.04	0.08	0.05	0.05
Total	99.81	100.24	99.78	99.00	98.81	100.19
			Structural Formula			
Si	1.876	1.919	1.944	1.945	1.933	1.899
Ti	0.005	0.004	0.005	0.017	0.011	0.011
Al	0.166	0.061	0.108	0.088	0.109	0.150
Cr	0.019	0.008	0.019	0.016	0.017	0.016
Fe^{2+}	0.190	0.195	0.190	0.212	0.200	0.203
Mn	0.003	0.005	0.004	0.004	0.005	0.005
Ni	0.002	0.000	0.000	0.003	0.000	0.000
Mg	1.738	1.833	1.694	1.687	1.689	1.699
Ca	0.027	0.017	0.022	0.011	0.026	0.022
Na	0.000	0.000	0.000	0.000	0.000	0.000
K	0.001	0.001	0.002	0.004	0.002	0.002
Total	4.027	4.043	3.988	3.987	3.993	4.008
En	88.89	89.63	88.87	88.32	88.23	88.32
Fs	9.72	9.52	9.96	11.09	10.44	10.54
Wo	1.39	0.85	1.17	0.59	1.34	1.14

Broad beam (=80 μm) was used. (s), small grains; (r), rim of crystal; (c), core of crystal.

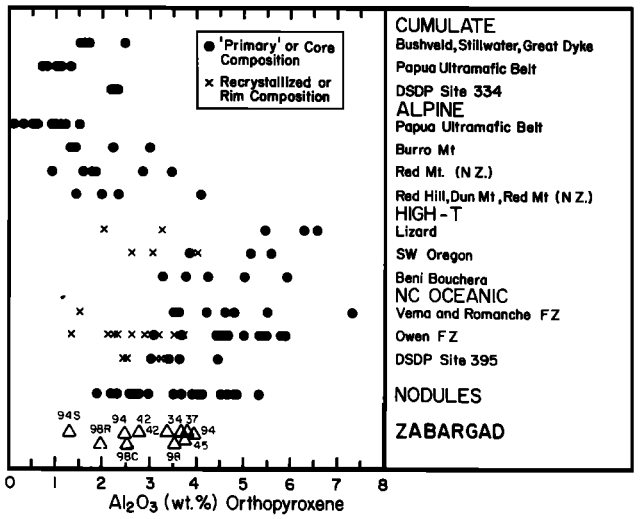

Fig. 7. Al_2O_3 content of orthopyroxenes from Zabargad peridotites, compared with that of peridotites from various settings, taken from Bonatti and Hamlyn [1981].

lization of pargasite can be estimated from experimental work by Boyd [1959], Spear [1981], Gilbert et al. [1982], and Robinson et al. [1982]. The melting temperature of pargasite ranges from 1040°C to 1060°C between 750 and 1500 bars P_{H_2O}. As discussed by Melson et al. [1972], extrapolation to higher P_{H_2O} would not raise the melting temperature much above 1100°C; therefore we consider this as the maximum temperature of pargasite crystallization in the Zabargad lherzolites. Magnesio-hornblende, which partially or totally replaced pyroxene and spinel in the amph-peridotites, probably crystallized at lower PT conditions.

Plagioclase

Plagioclase is generally absent in the Zabargad protogranular sp-lherzolites, except in a few cases where trace quantities of this phase were observed in thin section, rimming spinel crystals (Figure 4). In one such case (Z-37, Table 8) the plagioclase was found to be relatively sodic (An 55). This

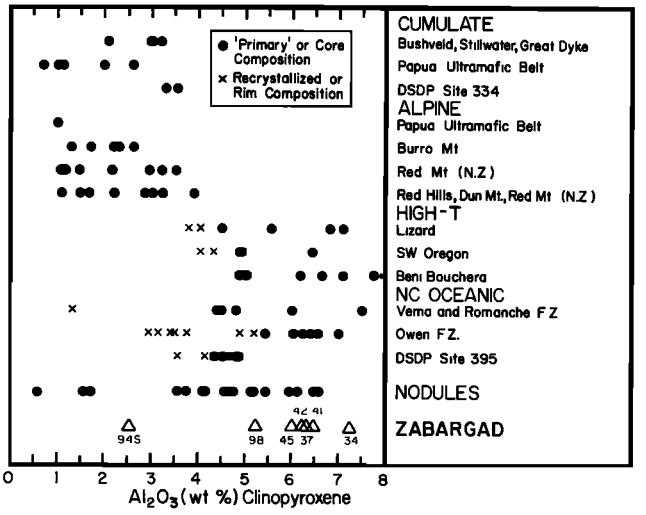

Fig. 8. Al_2O_3 content of clinopyroxenes from Zabargad peridotites, compared with that of peridotites from various settings, taken from Bonatti and Hamlyn [1981].

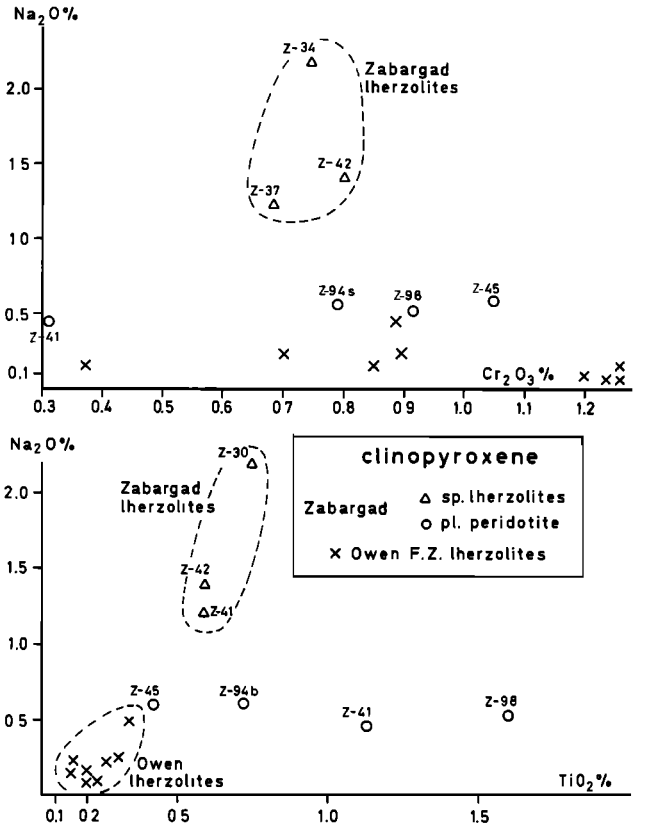

Fig. 9. Na2O versus Cr2O3 and TiO2 content in clinopyroxenes from Zabargad spinel lherzolites and plagioclase peridotites, compared with that of clinopyroxenes from the Owen Fracture Zone lherzolites, from Hamlyn and Bonatti [1980].

sodic composition might indicate involvement of cpx in the reactions which produced plagioclase, with Na being released by the cpx preferentially to Ca. In the pl-peridotite group, where plagioclase generally occurs in clusters surrounding spinel or in aggregates aligned along preferential bands, its composition is relatively calcic, ranging from An 80 to An 93 (Table 8).

Phlogopite

Trace quantities of phlogopite have been detected in some of the amph-peridotites and also in one sample of sp-lherzolite (Z-42). Two analyses (Table 9) indicate that these phogopites are relatively Ti-rich. Laboratory experiments have shown that phlogopite can be stable up to pressures ≈40 kbar and

TABLE 5. Temperatures of Equilibration for Some Zabargad Spinel Lherzolites and Plagioclase Lherzolites Estimated Using Wells [1977] Two-Pyroxene Geothermometry

Sample	Rock Type	Temperature, °C	
Z-37	sp-lherzolite	853	Av. 897°C
Z-34	sp-lherzolite	933	
Z-42	sp-lherzolite	904	
Z-45	pl-lherzolite	877	Av. 885°C
Z-95	pl-lherzolite	873	
Z-98	pl-lherzolite	905	

TABLE 6. Electron Probe Chemical Analyses of Spinels From Zabargad Peridotites

	sp-Lherzolite			amph-pl-Peridotite	pl-Peridotite	Gabbroic	
	Z-37	Z-34	Z- 42	Z-45	Z-69	Z-41a	Z-41b
TiO_2	0.09	0.42	0.02	0.16	0.30	0.05	0.08
Al_2O_3	56.98	57.80	58.00	31.42	40.10	61.40	56.50
Cr_2O_3	9.17	8.52	10.30	33.66	24.40	5.13	10.60
FeO	12.92	12.20	13.20	20.93	19.00	12.20	13.90
MnO	0.11	0.09	0.09	0.27	0.17	0.11	0.12
NiO	0.42	0.49	0.41	0.20	0.12	0.41	0.30
MgO	19.85	19.90	19.40	13.61	15.40	20.60	20.10
Total	99.54	99.42	101.42	100.25	99.49	99.90	101.60
			Structural Formula Based on Four Oxygens				
Ti	0.002	0.008	0.000	0.004	0.006	0.000	0.002
Al	1.747	1.769	1.755	1.090	1.339	1.84	1.708
Cr	0.189	0.175	0.209	0.783	0.547	0.103	0.215
Fe^{2+}	0.281	0.265	0.283	0.515	0.450	0.260	0.298
Mn	0.002	0.002	0.002	0.007	0.004	0.002	0.003
Ni	0.009	0.010	0.008	0.005	0.003	0.008	0.006
Mg	0.770	0.770	0.742	0.597	0.650	0.782	0.768
Total	3.000	3.000	3.000	3.000	3.000	3.000	3.000

temperatures close to 1200°C, above which it breaks down to garnet and other phases [Kushiro et al., 1967; Yoder and Eugster, 1954]. Therefore the phlogopite of the Zabargad peridotites could have formed under upper mantle conditions.

Apatite

Interstitial apatite, found in trace quantities in amph-peridotite Z-206, contains up to ≈5% chlorine. Apatite can form under upper mantle conditions [Watson, 1980].

Major Element Composition

The major element composition of samples of Zabargad peridotites was determined by standard X ray fluorescence methods with a Philips PW 1950 unit [Franzini et al., 1975; Leoni and Saitta, 1976]. FeO was determined by colorimetry, MgO by atomic adsorption spectrometry (AAS), and H_2O^+ gravimetrically.

The major elements composition of the Zabargad sp-lherzolites (Table 10) is very close to that of sp-lherzolites of mantle derivation tabulated by Maaloe and Aoki [1977] and to Ringwood's [1975] average pyrolite. The pl-peridotites (Table 11) tend to be richer in Ca and Al relative to the sp-lherzolites, with the enrichment being parallel to the increase in modal plagioclase. The amph-peridotites (Tables 12 and 13) do not show any significant difference relative to the sp-lherzolites except for an increase in K in the samples richer in amphibole and high P in a rock (Z-206) containing apatite.

Rare Earth Element Composition

Rare Earth Element (REE) analyses of Zabargad rocks (Table 14) have been performed by radiochemical neutron activation analysis (RNAA). Measurements were carried out by high-resolution gamma ray spectrometry, with Ge(Li) and pure Ge detectors (Ce, Nd, Tm, Gd). The chemical yield was controlled by reactivation techniques [Treuil et al., 1973; Ottonello, 1979; Joron and Ottonello, 1981]. The precision of the data can be estimated from the results of duplicated analyses (deviations from the mean in Table 14). The accuracy of the measurements is believed to be equal to the precision; values with a poor counting statistic have been omitted.

Protogranular sp-lherzolites (Z-34, Z-37 and Z-48) are essentially heavy REE (HREE) unfractionated relative to carbonaceous chondrites (Figure 12), have about twice the chondritic HREE content and are light REE (LREE) depleted. Z-94 (slightly tectonized and with some plagioclase) has a similar REE pattern and lower abundances. Z-37p (a pyroxene-rich layer within Z-37) has a REE pattern identical to the host peridotite but higher overall REE abundances, suggesting that the REE patterns of each single phase in Z-37 and Z-37p are similar and that differences in total abundance are due to modal mineralogy. Some samples display slightly positive Eu anomalies. The REE chemistry of these peridotites is similar to peridotites of some ophiolite complexes [Menzies and Allen, 1974; Loubet et al., 1975; Menzies et al., 1977;

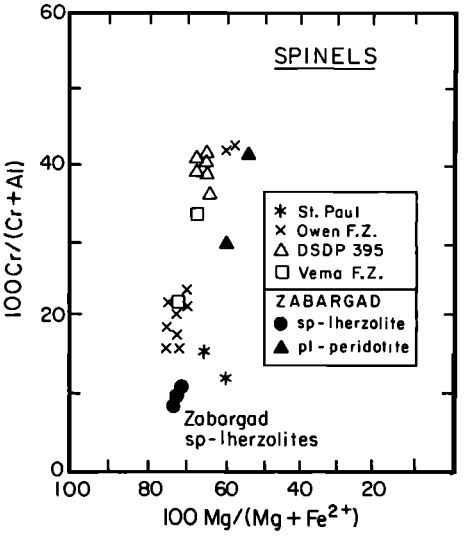

Fig. 10. Composition of spinels from Zabargad peridotites, compared with spinels from various oceanic ultramafics, from Bonatti and Hamlyn [1981].

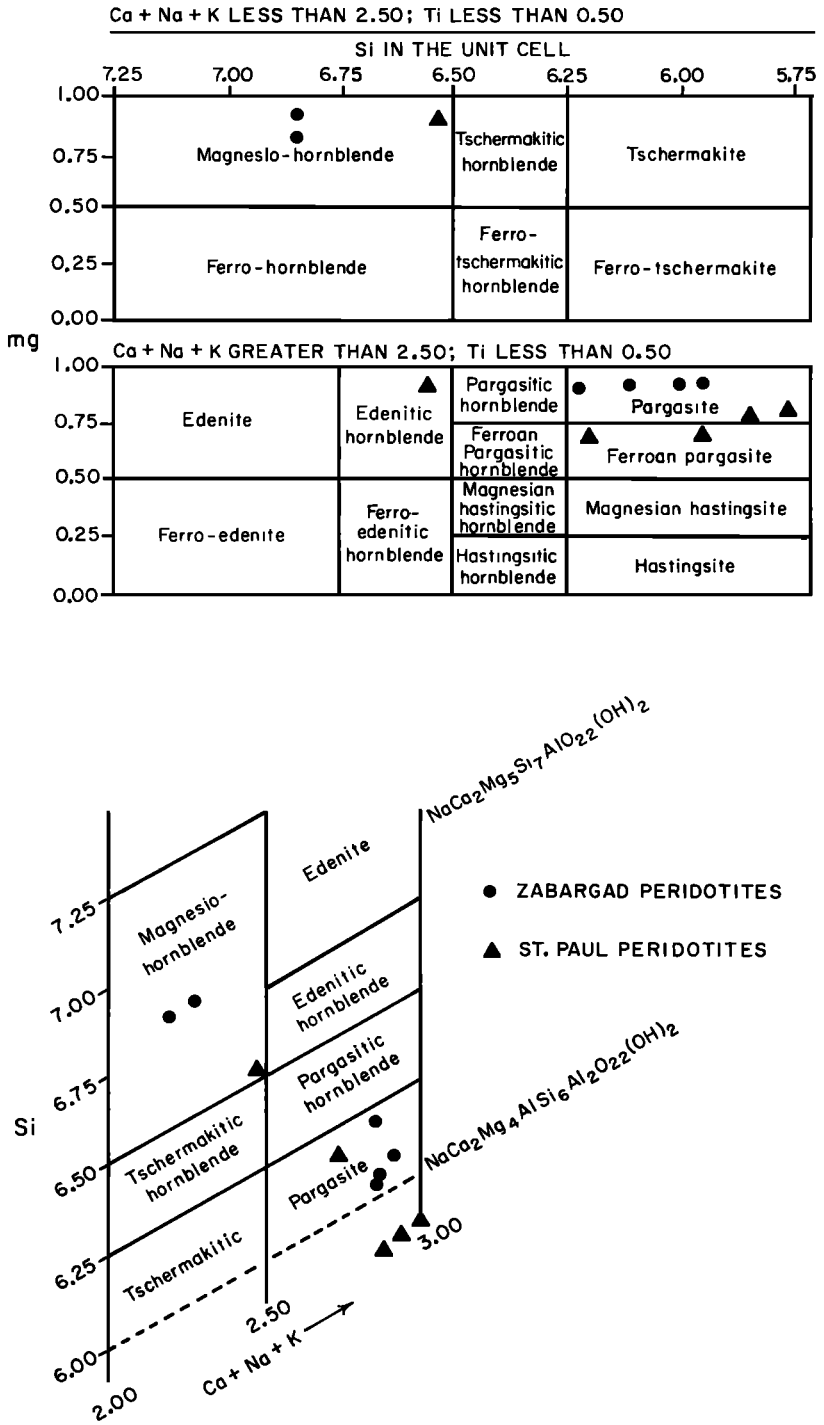

Fig. 11. Classification in terms of Si and Ca + Na + K (A), and in terms of Si and Ca + Na + K, mg and Ti (B), of amphiboles from the Zabargad peridotites compared with amphiboles from St. Paul peridotites analyzed by Melson et al. [1972]. Classification is after Leake [1968].

Ottonello et el., 1980b,1984b] and also to "recrystallized" assemblages in the Lizard peridotite body [Green, 1964; Frey, 1969].

The amph-peridotites are LREE enriched relative to chondrites (Figure 13). Among them, Z-35, Z-36, Z-204, and Z-205 display positive Eu anomalies and REE patterns with maxima at Ce or Nd (Z-205). The REE enrichment of these rocks is reminiscent of that found in peridotite nodules from alkali basalts [Nagasawa et al., 1969; Frey et al., 1971; Philpotts et al., 1972; Frey and Green, 1974; Ridley and Dawson, 1975; Shimizu, 1975] and from basanitic dikes [Wass and Rodgers, 1980]. Such an enrichment is usually ascribed to contamination by metasomatic fluids high in large ion lithophile elements (LIL) [Frey and Green, 1974; Shimizu, 1975; Ottonello, 1980; Wass and Rodgers, 1980; Bailey, 1982] with the contaminant being either interstitial to grain boundaries [Ottonello, 1980] or contained within the peridotitic minerals [Frey and Green, 1974].

TABLE 7. Electron Probe Chemical Analyses of Amphiboles From Zabargad Peridotites

	sp-Lherzolite			amph-Peridotite		
	Z-37	Z-42a	Z-42b	Z-35	Z-206a	Z-206b
SiO_2	41.81	43.00	43.50	43.70	48.60	48.40
TiO_2	4.49	1.73	1.79	3.53	0.06	0.05
Al_2O_3	12.46	14.40	14.50	12.70	8.34	8.21
Cr_2O_3	1.63	0.94	1.04	0.40	2.00	1.65
FeO	4.51	4.22	4.45	4.82	4.51	4.32
MnO	0.14	0.02	0.00	0.09	0.07	0.04
NiO	0.09	0.08	0.08	0.07	0.12	0.13
MgO	16.65	18.70	17.90	16.90	20.90	21.00
CaO	11.80	11.80	12.20	12.40	9.90	10.30
Na_2O	3.16	3.35	3.25	2.86	2.19	2.21
K_2O	0.90	0.90	1.09	0.91	0.45	0.37
Total	97.64	99.14	99.80	98.38	97.14	96.68
			Structural Formula, Based on 23 Oxygens			
Si	6.033	6.063	6.103	6.219	6.879	6.880
Ti	0.487	0.183	0.189	0.378	0.006	0.005
Al	2.119	2.393	2.398	2.130	1.391	1.375
Cr	0.186	0.105	0.115	0.045	0.224	0.185
Fe^{2+}	0.544	0.498	0.522	0.574	0.534	0.514
Mn	0.017	0.002	0.000	0.011	0.008	0.005
Ni	0.010	0.009	0.009	0.008	0.014	0.015
Mg	3.581	3.930	3.743	3.585	4.409	4.449
Ca	1.824	1.783	1.834	1.891	1.501	1.569
Na	0.884	0.916	0.884	0.789	0.601	0.609
K	0.166	0.162	0.195	0.165	0.081	0.067
Total	15.852	16.044	15.992	15.793	15.649	15.673

TABLE 8. Electron Probe Chemical Analyses of Plagioclase From Zabargad Peridotites

	sp-Lherzolite	amph-pl-Peridotite	pl-Peridotite		Gabbroic	
	Z-37	Z-45	Z-94	Z-98	Z-69	Z-41
SiO_2	52.40	46.48	46.30	47.00	48.10	44.40
TiO_2	0.00	0.00	0.00	0.00	0.05	0.00
Al_2O_3	30.59	33.40	34.10	34.90	32.10	35.50
Cr_2O_3	0.02	0.11	0.00	0.00	0.01	0.05
FeO	0.23	0.22	0.15	0.03	0.07	0.21
NiO	0.03	0.05	0.00	0.00	0.03	0.00
MgO	0.04	0.08	0.11	0.07	0.06	0.10
CaO	11.28	15.99	17.50	17.40	16.30	18.30
Na_2O	5.09	2.18	1.70	1.66	2.17	0.78
K_2O	0.05	0.04	0.04	0.04	0.05	0.05
Total	99.73	98.55	99.90	101.10	98.94	99.39
			Structural Formula, Based on 32 Oxygens			
Si	6.515	8.660	8.535	8.540	8.907	8.244
Ti	0.000	0.000	0.000	0.000	0.007	0.000
Al	6.547	7.335	7.409	7.474	7.006	7.769
Cr	0.003	0.016	0.000	0.000	0.001	0.007
Fe^{2+}	0.035	0.034	0.023	0.005	0.011	0.033
Ni	0.004	0.007	0.000	0.000	0.004	0.000
Mg	0.011	0.022	0.030	0.019	0.017	0.028
Ca	2.194	3.192	3.456	3.388	3.234	3.641
Na	1.792	0.788	0.608	0.585	0.779	0.281
K	0.012	0.010	0.009	0.009	0.012	0.012
Total	20.113	20.064	20.070	20.020	19.978	20.014
Ab	44.82	19.74	14.92	14.69	19.36	7.14
An	54.89	80.02	84.85	85.08	80.35	92.56
Or	0.29	0.24	0.23	0.23	0.29	0.30

TABLE 9. Electron Probe Chemical Analyses of Phlogopite From Zabargad Peridotites

	sp-Lherzolite Z-42	amph-Peridotite Z-35
	Oxide Percent	Oxide Percent
TiO_2	3.51	3.89
Cr_2O_3	0.92	0.34
MnO	0.00	0.09
FeO	3.82	4.51
NiO	0.18	0.16
SiO_2	37.50	38.60
K_2O	7.85	8.78
CaO	0.01	0.14
Na_2O	1.34	0.91
MgO	23.14	22.00
Al_2O_3	17.40	15.80
Total	95.67	95.26

La is about one order of magnitude higher in these rocks than in other Zabargad peridotites with similar Mg/(Mg + Fe^{+2}) ratio; the TiO_2 or La content of the amph-peridotites correlates inversely with Mg/ (Mg + ΣFe) (Figure 14). Among the rocks of this group, Z-206 has the highest overall REE content and lower (La/Sm) enrichment factor, probably related to its anomalous P_2O_5 content (Table 13) due to presence of apatite. REE data [Frey, 1970] of "pyroxene-type" (7-237) and "amphibole-type (18-900) sp-peridotite mylonite of St. Paul Rocks [Melson et al., 1967] are also reported in Figures 13 and 14 for comparison. The Zabargad amph-peridotites have Na_2O and K_2O contents comparable to St. Paul sample 18-900 but are lower in TiO_2 and H_2O^+, while 7-327 is lower in alkalies and has TiO_2 and H_2O^+ values comparable to the Zabargad rocks.

The pl-peridotites (except for Z-41) display an increase in REE content from La to Lu (Figures 15a and 15b) and are

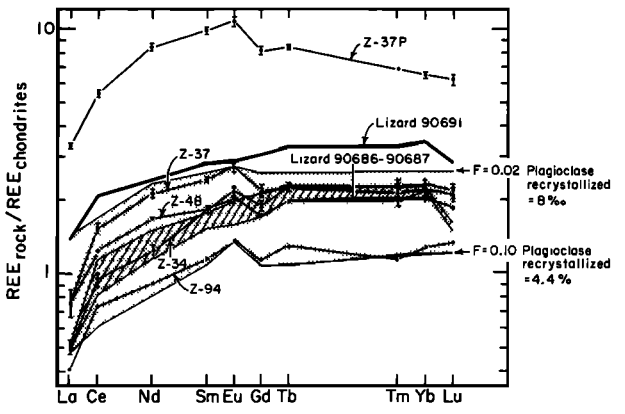

Fig. 12. Chondrite-normalized REE composition of protogranular sp-lherzolites (Z-34; Z-37; Z-48). Error bars represent deviations from the mean of duplicated analyses. Normalizing values are listed in Table 14. Sample Z-37p is a pyroxene-rich layer within Z-37. Z-94 contains plagioclase. REE compositions in recrystallized portions of the Lizard peridotite are also reported for comparison. Heavy line, recrystallized hydrous assemblage (samples 90680-90686 [Green, 1964; Frey 1969]. The shaded area includes compositional ranges of equilibrium partial melting residua (F = 2-10%) after recrystallization of 8-4.4% plagioclase. See text for further explanations.

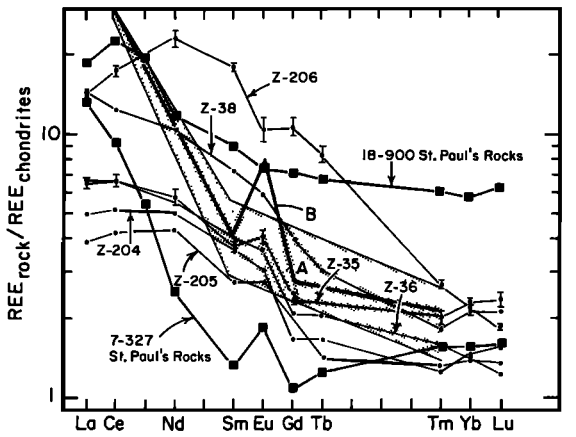

Fig. 13. Chondrite-normalized REE compositions of amph-peridotites. REE composition of samples 18-900 and 7-237 from St. Paul Rocks [Melson et al., 1967; Frey, 1970] are reported for comparison. The shaded area encloses REE compositions of H_2O vapor in equilibrium with incipient melting liquid produced during fusion at the cusp of a chondritic sp-peridotite source [from Mysen, 1979].

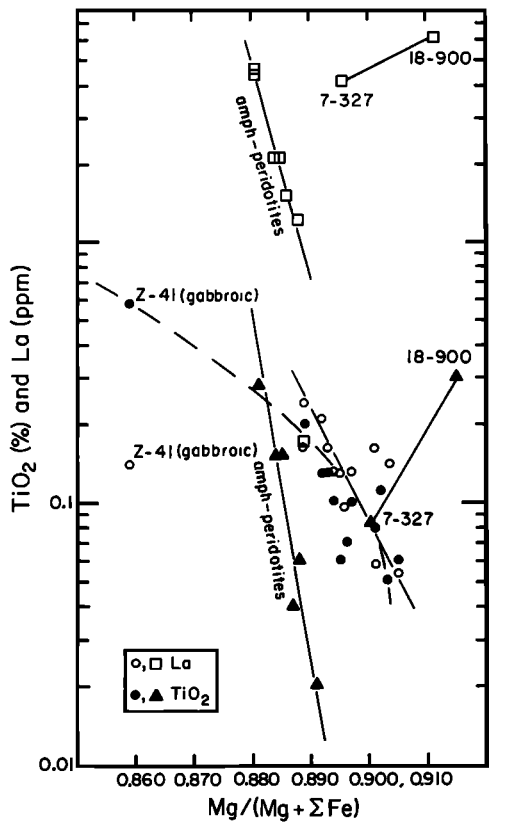

Fig. 14. La (open symbols) and TiO_2 (solid symbols) contents in Zabargad peridotites plotted against the Mg/(Mg + ΣFe) value. Squares and triangles refer to amph-peridotites; circles to sp-lherzolites and pl-peridotites. Samples 7-327 and 18-900 from St. Paul Rocks [Melson et al., 1967; Frey, 1970] are reported for comparison.

TABLE 10. Major Element Chemical Composition of Zabargad Protogranular Spinel Lherzolites

	Z-34	Z-37	Z-48	Z-1353	Z-1355	Z-37p	(Wherlite) Z -1323
SiO_2	44.02	44.40	44.16	45.07	45.62	48.09	42.66
TiO_2	0.13	0.20	0.13	0.15	0.14	0.68	0.02
Al_2O_3	3.70	4.01	3.66	4.01	3.87	7.02	1.80
Fe_2O_3	1.98	1.92	1.78	1.52*	1.47*	1.90	1.58*
FeO	6.63	6.75	6.85	7.51	7.51	4.20	8.04
MnO	0.14	0.14	0.14	0.15	0.15	0.11	0.15
MgO	39.19	38.19	39.10	36.84	36.69	25.49	40.32
CaO	3.06	3.29	3.03	3.26	3.28	10.53	3.19
Na_2O	0.34	0.34	0.34	0.35	0.33	1.01	0.38
K_2O	0.02	0.03	0.02	0.02	0.04	0.04	0.06
P_2O_5	0.00	0.01	0.03	0.01	0.01	0.01	0.91
H_2O^+	0.79	0.79	0.73	0.38	0.38	0.92	0.44
CO_2	-	-	0.088	-	-	0.140	-
	100.00	100.07	100.06	99.52	99.49	100.14	99.55
$\frac{100\,Mg}{(Mg+Fe^{2+})}$	91.4	91.0	91.1	-	-	91.5	-
$\frac{Mg}{(Mg+\sum Fe)}$	0.893	0.889	0.892	0.878	0.881	0.885	0.883

	Mean (excluding Z-37p Z-1323)	Maaloe and Aoki [1977] estimates		Dick and Fisher [1984]	Carter [1970]	Ringwood [1979]
		Continental sp-Lherzolite	Oceanic sp-Lherzolite	Computed Abyssal Peridotite	Kilbourne Hole Upper Mantle	Average Pyrolite
SiO_2	44.65	44.15	44.40	43.6	42.86	45.1
TiO_2	0.15	0.07	0.13	0.02	0.33	0.2
Al_2O_3	3.85	1.96	2.38	1.18	6.99	3.3
Fe_2O_3	1.89**	-	-	0.02	0.36	-
FeO	6.74**	8.29***	8.31***	8.20	8.97	8.0***
MnO	0.14	0.12	0.17	0.14	0.14	0.15
MgO	38.00	42.25	42.06	45.2	35.07	38.1
CaO	3.18	2.08	1.34	1.13	4.37	3.1
Na_2O	0.34	0.18	0.27	0.02	0.45	0.4
K_2O	0.03	0.05	0.09	-	0.0003	0.3
P_2O_5	0.01	0.02	0.06	-	-	0.02
H_2O^+	0.68	-	-	-	-	-
CO_2	-	-	-	-	-	-
Total	-	-	-	-	-	-
$\frac{100\,Mg}{(Mg+Fe^{2+})}$	91.2	-	-	-	87.5	-
$\frac{Mg}{(Mg+\sum Fe)}$	0.890	0.901	0.900	0.908	0.870	0.890

Composition of mantle-derived oceanic and continental spinel lherzolites from Maaloe and Aoki [1977] and Carter [1970], of computed average abyssal peridotites from Dick and Fisher [1984], and of average pyrolite [Ringwood, 1979] are included for comparison. Also shown are data for a pyroxenite band within Z-37 and for a wherlite. Data were obtained by XRF, AAS (MgO), colorimetric (FeO), and gravimetric (H_2O^+) methods.

*Fe_2O_3 as 15% FeO_{tot};

**Mean of three values (Z-34+Z-37+Z-48);

***Total iron as FeO.

TABLE 11. Major Element Composition of Zabargad Plagioclase Peridotites

	Z-202	Z-94	Z-92	Z-137	Z-68	(Gabbroic) Z-41
SiO_2	43.52	43.89	45.32	45.44	46.79	45.91
TiO_2	0.08	0.10	0.06	0.08	0.17	0.58
Al_2O_3	2.98	3.99	4.41	5.67	9.55	13.05
Fe_2O_3	1.44	1.98	1.44	1.36	2.23	1.87
FeO	6.83	6.43	6.37	6.93	4.37	3.10
MnO	0.13	0.13	0.13	0.14	0.12	0.10
MgO	41.71	39.87	38.51	35.64	28.82	19.15
CaO	2.12	2.61	2.73	3.33	6.99	14.98
Na_2O	0.24	0.21	0.30	0.43	0.66	0.51
K_2O	0.02	0.02	0.02	0.01	0.02	0.02
P_2O_5	0.00	0.00	0.00	0.00	0.00	0.00
H_2O^+	0.94	0.76	0.70	0.55	0.78	0.73
CO_2	0.035	-	0.036	-	0.120	0.071
Total	100.05	99.99	100.03	99.58	100.62	100.07
$\frac{100\,Mg}{(Mg+Fe^{2+})}$	91.6	91.7	91.5	-	92.1	90.8
$\frac{Mg}{(Mg+\Sigma Fe)}$	0.901	0.897	0.899	0.887	0.889	0.859

Modal plagioclase content increases from left to right.

LREE depleted relative to chondrites. A small Eu anomaly is apparent in some samples (Z-81 and Z-82, Figure 15a; Z-202, Figure 15b); the Eu anomaly is particularly large in Z-203a (Figure 15a), a plagioclase-rich segregation within Z-203. The REE composition of these rocks is similar to that of some oceanic gabbroic rocks [Kay et al., 1970; Shih, 1972; Shih and Gast, 1971; Schubert, 1972; Masuda and Jibiki, 1973; Dostal and Muecke, 1977].

Transition Element Composition

The Cr, Co, Ni, and Sc contents of the Zabargad peridotites, determined by instrumental neutron activation analysis [Treuil et al., 1973], are presented in Table 15. The enrichment factors (ef) of transition metals Sc, Ti, Cr, Mn, Fe, Co, Ni over the mean composition of CH carbonaceous chondrites, plotted versus element atomic numbers, are shown

TABLE 12. Major Element Chemical Composition of Zabargad Plagioclase-Containing Amphibole Peridotites

	Z-82	Z-201	Z-45	Z-81	Z-203	(pl-Rich Zone in 203) Z-203a
SiO_2	43.61	43.36	44.42	43.24	43.61	40.37
TiO_2	0.01	0.05	0.06	0.10	0.11	0.15
Al_2O_3	3.25	3.25	3.10	4.45	4.46	21.28
Fe_2O_3	3.85	1.55	1.03	2.00	1.30	2.12
FeO	4.98	6.68	6.74	6.51	6.64	4.16
MnO	0.14	0.13	0.12	0.14	0.14	0.09
MgO	40.70	41.85	41.10	39.43	40.31	23.50
CaO	2.19	1.96	2.52	2.77	2.32	6.04
Na_2O	0.19	0.19	0.13	0.20	0.23	1.24
K_2O	0.01	0.02	0.01	0.01	0.01	0.05
P_2O_5	0.00	0.00	0.00	0.00	0.00	0.00
H_2O^+	1.02	0.95	0.76	1.15	0.88	1.00
CO_2	0.038	-	0.046	0.042	0.061	-
Total	99.99	99.99	100.04	100.04	100.07	100.00
$\frac{100\,Mg}{(Mg+Fe^{2+})}$	93.6	91.8	91.6	91.5	91.6	90.9
$\frac{Mg}{(Mg+\Sigma Fe)}$	0.896	0.903	0.905	0.894	0.902	0.874

Modal amphibole and plagioclase contents increase from left to right.

TABLE 13. Major Element Chemical Composition of Zabargad Amphibole Peridotites

	Z-35	Z-38	Z-36	Z-1348	Z-1347	Z-1481
SiO_2	43.36	46.25	44.21	45.61	45.90	45.64
TiO_2	0.15	0.28	0.15	0.15	0.14	0.05
Al_2O_3	3.57	3.06	4.13	3.92	3.93	3.87
Fe_2O_3	2.14	2.35	1.94	1.47	2.76	1.32
FeO	7.30	5.74	6.98	7.51	6.51	6.73
MnO	0.16	0.14	0.15	0.14	0.15	0.14
MgO	39.13	32.63	37.68	36.45	36.01	38.47
CaO	2.76	7.84	3.13	3.24	3.26	2.76
Na_2O	0.45	0.56	0.53	0.37	0.40	0.17
K_2O	0.10	0.05	0.13	0.02	0.05	0.01
P_2O_5	0.02	0.01	0.01	0.01	0.01	0.00
H_2O^+	0.86	1.10	0.95	0.65	0.88	0.49
CO_2	0.086	0.070	0.038	-	-	-
Total	100.09	100.08	100.03	99.54	100.00	99.65
$\frac{100\,Mg}{(Mg+Fe^{2+})}$	90.5	91.0	90.6	-	90.7	-
$\frac{Mg}{(Mg+\Sigma Fe)}$	0.884	0.881	0.885	0.880	0.876	0.897
	Z-1346	Z-204	Z-205	Z-1326	Z-206	Z-1354
SiO_2	46.84	43.28	43.92	46.93	42.11	52.33
TiO_2	0.15	0.04	0.06	0.15	0.02	0.45
Al_2O_3	4.06	2.44	2.74	3.99	1.98	5.25
Fe_2O_3	1.59	1.97	2.12	1.38	1.65	0.95
FeO	8.08	7.55	7.11	7.05	7.50	4.84
MnO	0.15	0.15	0.14	0.13	0.14	0.13
MgO	34.44	41.21	40.20	35.44	40.99	20.44
CaO	3.33	2.02	2.22	3.43	3.45	12.64
Na_2O	0.37	0.39	0.42	0.44	0.46	1.48
K_2O	0.04	0.08	0.11	0.09	0.08	0.13
P_2O_5	0.01	0.01	0.01	0.02	0.78	0.06
H_2O^+	0.35	0.86	0.95	0.52	0.73	0.91
CO_2	-	-	0.080	-	0.060	-
Total	99.41	100.00	100.00	99.57	99.95	99.61
$\frac{100\,Mg}{(Mg+Fe^{2+})}$	-	90.7	91.0	-	90.7	-
$\frac{Mg}{(Mg+\Sigma Fe}$	0.866	0.887	0.888	0.884	0.891	0.865

Modal amphibole content increases from left to right.

in Figure 16. When normalized to CH carbonaceous chondrites, or C1 subtype carbonaceous chondrites [Langmuir et al., 1977], the transition elements from Sc to Ni behave as a coherent group. (The chemical composition of C1 subtype carbonaceous chondrites is very similar to that of the sun as far as condensable elements are concerned. The normalizing factors in Figure 16 are the mean compositions of CH chondrites comprising the C1, C2, C3 subgroups.) The ef in the analyzed samples decreases almost regularly by more than two orders of magnitude with increasing atomic number. This ef versus Z relationship is particularly regular between Cr and Co in the sp-lherzolites: it shows discontinuities in the Ti region in the other peridotite groups.

Discussion

Origin of the Protogranular Spinel Lherzolites

The Zabargad peridotites are clearly derived from the upper mantle. The arguments supporting this statement are particularly stringent for the protogranular sp-lherzolite group and can be summarized as follows: (1) The mineral assemblage of these rocks indicated equilibration within the PT stability field of spinel lherzolite facies [Green and Ringwood, 1967; Green and Hibberson, 1970; O'Hara, 1968; O'Hara et al., 1971], that is, at pressures higher than about 9 kbar corresponding to a depth greater than about 30 km. (2) The mineral chemistry

TABLE 14. REE Composition of Zabargad Peridotites.

	sp-Lherzolite		
	Z-34	Z-37	Z-48
La	0.16±0.01	0.24±0.03	0.21
Ce	0.75±0.05	1.19±0.05	0.99
Nd	0.71±0.04	1.22±0.04	0.98
Sm	0.33±0.03	0.44±0.01	0.334
Eu	0.155±0.001	0.112±0.002	0.102
Tm	0.078±0.002	0.069±0.009	0.069
Yb	0.4 0±0.0	0.415±0.005	0.376
Lu	0.074±0.004	0.07±0.001	0.063

	pl-Peridotite				Gabbroic	
	Z-202	Z-94	Z-92	Z-68	Z-41	Z-37p
La	0.164	0.131	0.14±0.01	0.172	0.141	1.055±0.005
Ce	0.66	0.57	0.39±0.03	1.12	1.58	4.3±0.1
Nd	0.53	0.53	0.36±0.02	1.39	2.76	4.85±0.07
Sm	0.181	0.21	0.14±0.002	0.584	1.187	1.80±0.05
Eu	0.089	0.096	0.076±0.004	0.268	0.481	0.77±0.02
Cd	n.d.	0.29	n.d.	n.d.	1.32	2.11±0.03
Tb	0.053	0.066	0.06	0.221	0.265	0.425±0.005
Tm	n.d.	0.038	0.051±0.003	n.d.	0.116	0.228
Yb	0.231	0.24	0.325±0.025	2.15	0.663	1.21±0.01
Lu	0.045	0.045	0.06±0.01	0.405	0.115	0.21±0.01

	amph-pl-Peridotites					
	Z-82	Z-201	Z-45	Z-81	Z-203	Z-203a
La	0.096	0.14±0.01	0.053	0.132	0.06±0.01	0.19±0.02
Ce	0.39	0.36±0.015	0.315	0.63	0.29±0.05	0.86±0.04
Nd	0.46	0.33±0.001	0.148	0.224	0.23±0.0	0.2±0.01
Eu	0.072	0.057±0.003	0.060	0.105	0.10±0.01	0.23±0.01
Gd	n.d.	n.d.	n.d.	n.d.	n.d.	0.32
Tb	0.048	0.046±0.004	0.047	0.075	0.10±0.01	0.069±0.001
Tm	0.040	0.039±0.003	0.038	0.057	0.15±0.01	0.087
Yb	0.240	0.25±0.01	0.238	0.372	0.97±0.0	0.51±0.01
Lu	0.045	0.05±0.002	0.049	0.075	0.195±0.015	0.11±0.01

	amph-Peridotites						Normalizing Values
	Z-35	Z-38	Z-36	Z-204	Z-205	Z-206	
La	2.08±0.07	4.65	2.13	1.585	1.24	4.46±0.24	0.32
Ce	5.2±0.25	9.74	5.27	4.09	3.38	13.77±0.52	0.787
Nd	3.4±0.1	6.125	3.27	2.875	2.51	13.34±0.98	0.580
Sm	0.69±0.01	1.36	0.73	0.695	0.5	3.34±0.03	0.185
Eu	0.285±0.015	0.420	0.262	0.213	0.197	0.74±0.08	0.071
Cd	0.59	1.03	0.54	0.43	n.d.	2.74±0.18	0.256
Tb	0.115±0.005	0.149	0.102	0.076	0.071	0.42±0.03	0.050
Tm	0.066±0.004	0.06	0.052	0.044	0.043	0.090±0.002	0.033
Yb	0.43±0.01	0.396	0.261	0.276	0.273	0.410±0.000	0.186
Lu	0.080±0.005	0.072	0.042	0.053	0.046	0.061±0.001	0.034

Data expressed as ppm. Deviations from the mean duplicated analyses are also reported (2 sigma values); n.d., not determined.

of the major phases (Fo content of olivine, Al and Cr content of pyroxene, Cr/Al ratio of spinel, etc.) supports crystallization under upper mantle conditions. The chemistry of pargasite and phlogopite, contained in trace amounts in some of the sp-lherzolites, is also consistent with an upper mantle origin. (3) Protogranular or coarse-mosaic textures, as displayed by the Zabargad sp-lherzolites, are typical of mantle-derived peridotites [Mercier and Nicolas, 1975; Harte, 1977]. Lack of cumulus textures also suggest a subcrustal origin. (4) Major elements, transition elements, and REE chemistry of the sp-lherzolites are all consistent with upper mantle origin for these rocks.

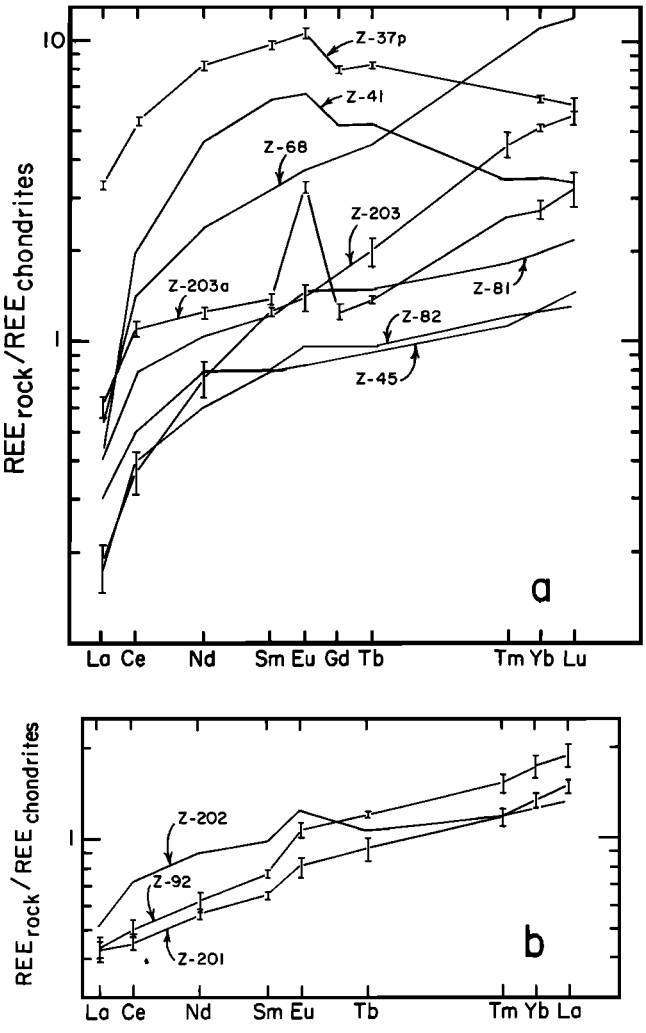

Fig. 15. Chondrite-normalized REE compositions of pl-peridotites. Z-203a is a plagioclase-rich segregation within Z-203.

The major element composition of the Zabargad sp-lherzolites is compared (Table 10) with average compositions of oceanic and continental sp-lherzolites compiled by Maaloe and Aoki [1977] and with the pyrolite composition of Ringwood [1975]. In terms of major elements, no significant and systematilc differences between oceanic and continental mantle-derived sp-lherzolite are apparent, except a slightly lower Ca content of the oceanic lherzolites [Maaloe and Aoki, 1977]. However, serpentinization may affect the major element chemistry and make an evaluation of these data difficult, particularly since Ca is one of the elements which may be affected. The Zabargad sp-lherzolites, not affected by serpentinization, contain slilghtly more Ca and Al and a slightly lower Mg/(Mg + ΣFe) ratio than oceanic peridotites (Figure 17) and of continental and oceanic sp-lherzolites of Maaloe and Aoki [1977]; however, they contain definitely more Ca, Al, Na, and K than Dick and Fisher's [1984] computed oceanic peridotites (Table 10); that is, they appear to be less "residual". Actually, some of the sp-lherzolites, such as sample Z-37, show a relatively low Mg/(Mg + ΣFe) ratio, a modal composition (Table 1) nearly coincident with undepleted upper mantle estimates [Carter, 1970], and a major element composition close to that of Ringwood [1975] pyrolite. Moreover, the spinel chemistry of these samples, particularly the very low Cr/(Cr + Al) ratio (Figure 9), suggests that they were not subjected to significant partial melting. This assumes that during partial melting, Cr and Mg partition with the solid and Al with the melt, so that spinel in undepleted peridotites is Al-rich but becomes more chromiferous with the degree of partial melting [Irvine, 1967; Dick, 1977; Jaques and Green, 1980; Dick and Fisher, 1984; Dick and Bullen, 1984]. Similar inferences can be derived from the high Al content of cpx and opx in the sp-lherzolites [Dick, 1977; Jaques and Green, 1980]. Thus some of the Zabargad sp-lherzolites approach undepleted upper mantle as far as modal and major element composition and mineral chemistry are concerned.

The composition of the Zabargad sp-lherzolites is compared in Figures 16 and 18 with estimates of solar abundance and mean composition of Cl subgroup carbonaceous chondrites [Ross and Aller, 1976; Ringwood, 1979; Wood, 1979]. Co, Ni, and Fe, together with alkalies, phosphorous, carbon, and oxygen, are the elements that most deviate from solar and Cl chondrite compositions. The observed depletions in third-period transition elements follow predictions by Ringwood [1966a,b, 1975, 1979] concerning the content of the earth's mantle in siderophile elements. As noted by Langmuir et al. [1977], the observed fractionation is caused neither by an early stage of intense partial melting in the mantle (in which case Ti would be more depleted than Ni) nor by continental crust segregation. Rather, it is due to fractionation during condensation or accretion from the solar nebula or to fractionation during core separation.

The fractionation should have been determined primarily by the siderophile tendency of the elements [Ringwood, 1979] combined with the effect of the gravitational field. These effects were probably enhanced by the effect of pressure on the crystal field stabilization energy (CFSE) of transition elements in silicate solid phases. The CFSE increases with pressure/depth in the mantle due to contraction of metal-ligand interatomic distances [Burns, 1970]. This effect, particularly evident for elements with high CFSE (i.e., Co^{2+} and Ni^{2+} in octahedral coordination), should have resulted in composiional gradients in the mantle, with the upper mantle being depleted preferentially in high CFSE elements. The observed depletion of alkalies in upper mantle rocks compared to solar system estimates could be due to their volatility [Ringwood, 1979]. However, the depletion in alkalies, phosphorous, and La in some of the Zabargad lherzolites could be also due to minor partial melting, probably related to adiabatic decompression during upwelling.

In order to test this hypothesis we have plotted the Zabargad ultramafic compositions in a di-q-ol-pl normative tetrahedron (Figure 19), where the experimental phase boundaries for the fo-an-di-SiO_2 system at 10 kbar under anhydrous conditions [Presnall et al., 1979] are also shown. Most of the Zabargad samples plot along a trend connecting the field of the liquid with that of a melting residuum made of ol + opx. This trend is close to the line connecting sp-lherzolite sample Z-37 with pyroxenitic vein Z-37p occurring in the same rock. Z-37p is shifted slightly relative to the invariant point T-1 for the ol-en-di-sp association (Figure 19). Similar relationships have been noted in the Baldissero Alpine peridotites, where the shift of the liquid composition from the T-1 invariant point has been ascribed to the abundance of the Cr end-member in the spinel field [Sinigoi et al., 1980, 1983].

The normative composition of the Zabargad peridotites is projected from the di apex of the tetrahedron onto the ol-pl-SiO_2 plane (Figure 20), in order to show the shift of the invariant point with pressure in the range 1 atm - 20 kbar. The melt changes with increasing pressure from quartz tholeiite (composition within the normative tetrahedron hy-pl-di-q) to olivine tholeiite (within hy-pl-di-ol space). At about 9 kbar the liquid composition plots at an invariant point in a zone of transition between the spinel and plagioclase

TABLE 15. Transition Element Composition of Zabargad Peridotites

	sp-Lherzolite			pl-Peridotite					
	Z-34	Z-37	Z-48	Z-202	Z-94	Z-92	Z-68	Z-41	Z-37p
Cr	2500	2270	2506	2569	2695	2587	2834	2887	1937
Co	110	107	106	108	106	97	71	53	76
Ni	2043	1891	2035	2199	2056	1953	1406	1084	2094
Sc	14	14	13	11	12	14	22	48	33

	amph-pl-Peridotite					
	Z-82	Z-201	Z-45	Z-81	Z-203	Z-203a
Cr	2567	2579	2808	2596	2553	1160
Co	109	109	105	109	103	87
Ni	2158	2182	2096	2148	1941	1064
Sc	11	10	12	14	30	29

	amph-Peridotite					
	Z-35	Z-38	Z-36	Z-204	Z-205	Z-206
Cr	2529	4329	2516	2865	2599	2574
Co	1084	87	100	107	100	106
Ni	1933	1500	1824	1974	1766	2195
Sc	12	20	13	11	11	9

Values are expressed in parts per million.

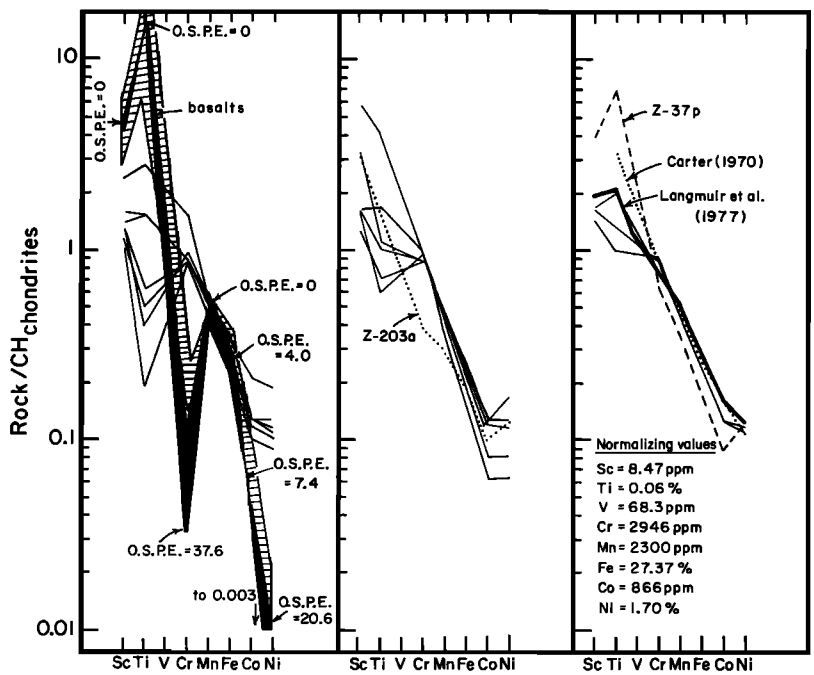

Fig. 16. Transition element enrichment factors (ef) in Zabargad peridotites (solid lines) with respect to CH chondrites. The normalizing values are labeled; values of octahedral site preference energy (O.S.P.E.) are also listed [Burns, 1970] for the different elements. Estimated ef derived for an average undepleted upper mantle composition according to Carter [1970] (dotted line) and Langmuir et al. [1977] for unfractionated basalts (diagonally patterned area) is compared with the composition of Zabargad basalt dikes (solid area).

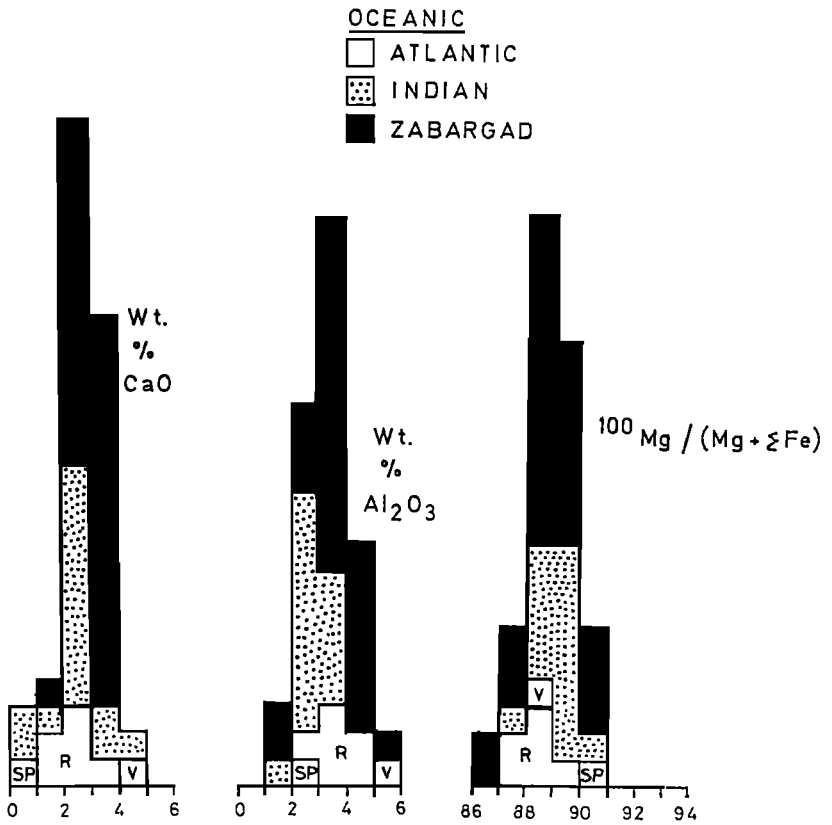

Fig. 17. CaO, Al2O3, and 100 Mg/(Mg + ΣFe) of Zabargad peridotites compared with peridotites from the ocean basins and from some ophiolite complexes. R, Romanche Fracture Zone; V, Vema Fracture Zone; SP, St. Paul Rocks.

stability fields for peridotite assemblages [Presnall et al., 1979]. The solidus of peridotite is depressed in this PT (≈9 kbar; 1300°C) region, and the cusp in the solidus acts as a thermal buffer so that the melting process depends on upwelling rate and degree of adiabaticity [Presnall et al., 1979]. According to Presnall et al., peridotite partial melting at the 9-kbar cusp results in the simultaneous depletion of spinel and diopside, leaving a residuum consisting of 87% olivine and 13% enstatite. The peritectic melting equation proposed by Presnall et al. is

$$.00954 \text{ res.} + 0.01957 \text{ liq.} = 0.00301 \text{ sp} + 0.01180 \text{ en} + 0.01430 \text{ di} \quad (1)$$

If the line joining the 9 kbar liquid with the Zabargad sp-lherzolites (Figure 19) is extended, it will meet the fo-en edge at a composition close to that of the suggested residuum. It appears, therefore, that, reasoning in terms of major element chemistry, the Zabargad sp-lherzolites range from undepleted (i.e., Z-37) to slightly depleted.

Equation (1) can be transformed and made suitable for trace element distribution modeling [Ottonello et al., 1984a,b], so that both major and trace elements can be treated within the same self-consistent framework. Transition elements and REE can be evaluated conveniently in terms of ternary fractionation diagrams Ni-Co-Sc and La-Sn-Lu, respectively, [Ottonello et al., 1984a,b]. Sc-Co-Ni fractionation trends in melt and residue for different degrees of melting (Figure 21) were obtained with different sets of partition coefficients appropriate to different temperatures during melting (1, T = 1200°C; 3, T = 1350° C). The distribution model and the choice of appropriate partition values are discussed by Ottonello et al. [1984a]. The melting case evaluated in Figure 21a pertains to fusion of a sp-peridotite source with modal composition consistent with upper mantle estimates [Carter, 1970] and melting proportions appropriate for the melting at the cusp event [Presnall et al., 1979; Ottonello et al., 1984a, b]. In Figure 21 the source is more pyroxene-rich, and the melting coefficients lead to a less pronounced production of olivine throughout the peritectic melting reaction. In both cases the composition of Zabargad peridotites has been normalized to Z-37 sp-lherzolite, taken as representative of upper mantle not subject to a melting event. Comparing Figures 21a and 21b, it appears that the melting dynamics and the modal composition-melting proportion of the solid do not significantly affect the Ni-Co-Sc fractionation of the melting residue. These parameters, as well as temperature, affect markedly the relative Ni-Co-Sc proportions in the resulting liquids. Comparing the calculated and observed fractionation trends (Figure 21), some of the Zabargad sp-lherzolites could be regarded as residue from small degrees of partial melting.

Comparison of calculated La-Sm-Lu ratios of the Zabargad rocks (Figure 22) shows that some of the sp-lherzolites plot in a region of the diagram compatible with their being residue of a low degree of melting. Sample Z-37p, a pyroxenitic vein cutting through sp-lherzolite Z-37, has a La-Sm-Lu ratio compatible with it being a fractional melting liquid.

We conclude that some of the Zabargad sp-lherzolites approach undepleted upper mantle material. Some other sp-lherzolites could have undergone a small degree of partial melting, at least in terms of REE and transition element chemistry.

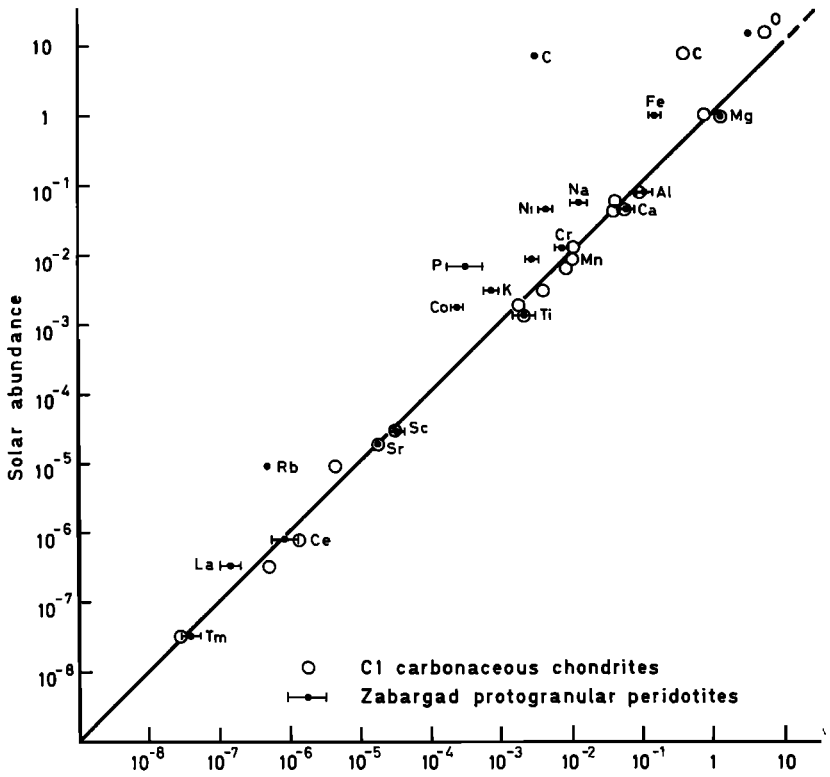

Fig. 18. Elemental abundances in Zabargad protogranular sp-lherzolites compared with abundances in the sun. A comparison between Cl carbonaceous chondrites and the sun is also shown. Values are expressed as atoms per silicon atom.

Origin of the Plagioclase Peridotites

Plagioclase peridotites similar to those found at Zabargad are known from several ophiolite complexes and from oceanic areas such as the Romanche Fracture Zone [Bonatti and Honnorez, 1976; Dick and Bullen, 1984] and St. Paul Rocks in the equatorial Atlantic [Melson et al., 1972]. The Zabargad pl-peridotites could have originated by crystallization of a small fraction of trapped melt, which could either (1) be consanguineous with the sp-lherzolite or (2) result from addition of an exotic melt component.

The first hypothesis implies incomplete expulsion and subsequent in situ crystallization of a liquid produced by incipient melting of the sp-lherzolite. This hypothesis was favored by Jacobsen et al. [1984] for the Trinity ophiolite pl-peridotites, based on isotopic data, and by Hamlyn and Bonatti [1980] for pl-lherzolites from the western Indian Ocean. The second hypothesis, which implies introduction of an exotic melt fraction presumably generated at a deeper level by a source similar in composition to the sp-lherzolite, has been suggested to explain the origin of some ophiolitic and oceanic pl-peridotites [Nicolas and Dupuy, 1984; Dick and Bullen, 1984].

Most of the Zabargad pl-peridotites plot along the tie-line between undepleted sp-lherzolite Z-37 and pyroxenitic vein Z-37p in the normative diagram of Figure 19. They are more scattered in the projection from the di apex diagram (Figure 20). According to the Sc-Co-Ni fractionation diagram (Figure 21) the pl-peridotites could be mixtures of liquid and residue. Their REE data cannot be interpreted by a single unambiguous model. Most of the samples plot outside the range consistent with equilibrium melting residue in the La-Sm-Lu diagram of Figure 22. Some do and some do not display a Eu anomaly (Figures 15a and 15b). On the basis of major and trace element composition, either the "consanguineous" or the "exotic" melt hypothesis could explain the pl-peridotites.

A possible objection to the "consanguineous melt" hypothesis is that if the melt fraction which produced the pl-peridotites was generated by partial melting at the "cusp" of the sp-lherzolites, a temperature of about 1250°C would have been required. Such temperatures upon further ascent would have led to substantial reequilibration within the pl-lherzolites facies stability field. This is contrary to observations, in so far as protogranular sp-lherzolites are preserved and abundant at Zabargad, some only showing incipient reequilibration in the form of thin Na-rich plagioclase rims on spinel, different in composition from the Ca-rich plagioclase of the pl-peridotites.

The "exotic melt" hypothesis is compatible with evidence suggesting that the formation of the pl-peridotites was limited to structural planes within the Zabargad sp-lherzolite body, in so far as the pl-peridotites tend to show porphyroclastic or cataclastic textures, contrary to the sp-lherzolites. If the exotic melt injections occurred along preferential structural planes, and acted as localized heat sources, some reequilibration might have taken place in the surrounding rocks, with localized secondary melting of low-T melting components, i.e., breakdown of clinopyroxene and/or recrystallization of Na-rich to Na-poor clinopyroxene, and of Al-rich to Cr-rich spinel. However, these processes would not affect sp-lherzolites farther removed from the injections.

The fact that Wells' [1977] two-pyroxene geothermometry gives similar temperatures for the sp-lherzolites and the pl-peridotites (Table 5) may indicate slow cooling of the pl-peridotite from quasi-solidus temperatures to final equilibration temperatures similar to those of the sp-lherzolites. While at present we favor incorporation of an exotic melt as the explanation for the Zabargad pl-peridotites,

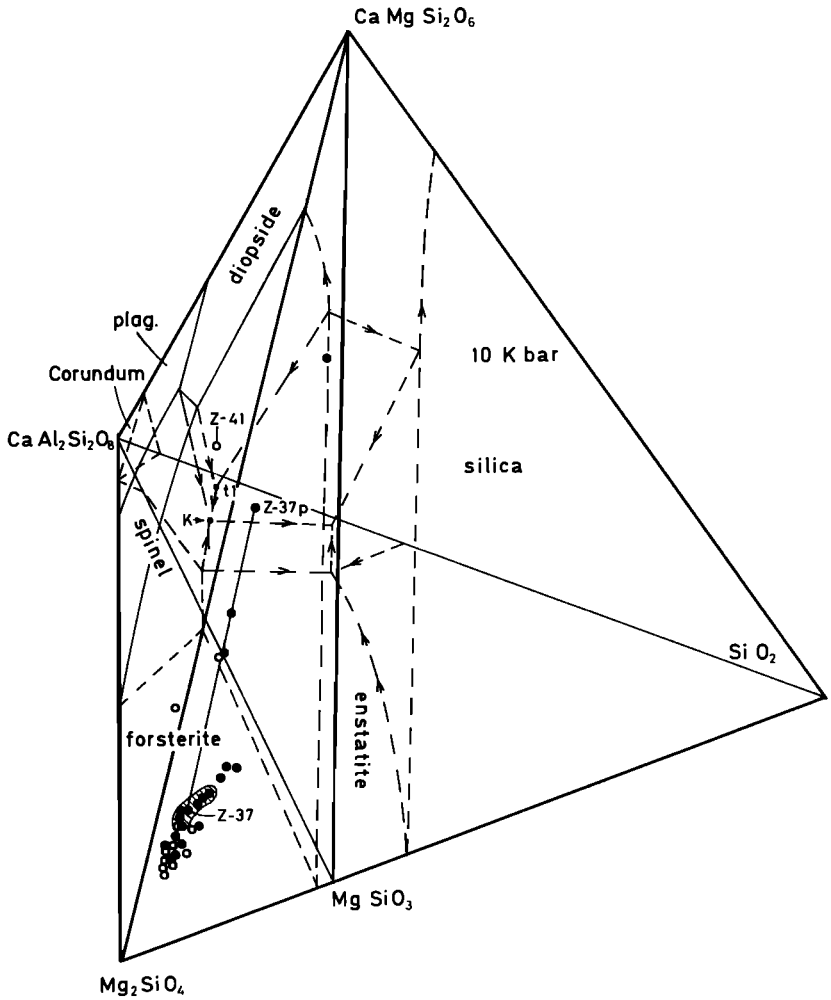

Fig. 19. ol (fo + fa) - di (wo + en + fs) - pl (ab + an) - q (SiO_2) CIPW normative composition of Zabargad rocks plotted in the Mg_2SiO_4 - $CaMgSi_2O_6$ - $CaAl_2Si_2O_6$ - SiO_2 tetrahedron. Liquidus phase relations (weight proportions) are at 10 kbar P total, according to Presnall et al. [1979]. K, isobaric invariant point for the an-sp-en-di assemblages; tl, isobaric invariant point for the ol-en-di-sp assemblage. Solid circles represent plagioclase-free peridotites; open circles are pl-peridotite. No distinction is made between amphibole-bearing and amphibole-free peridotites. The dashed area encloses the Zabargad protogranular sp-lherzolites. A tie-line connects protogranular sp-lherzolite Z-37 with the pyroxenitic vein Z-37p crossing through the same rock.

further field and analytical work is required to settle this matter.

Origin of the Amphibole Peridotites and Mantle Metasomatism

The presence at Zabargad of amph-peridotites (containing >2% relatively large magnesio-hornblende laths which partly or totally replace pyroxenes) suggests a situation similar to that of other known mantle-derived ultramafic bodies or nodules where amph-peridotites are associated with sp-lherzolites. Examples are St. Paul Rocks in the equatorial Atlantic [Melson et al., 1972; Roden et al., 1984]; the Causon complex in France [Conquere, 1971]; mantle inclusions at Grand Canyon in the United States, New Zealand, and Australia [Best, 1974], as well as nodules at Ataq, South Yemen [Varne, 1970], Nunivak Island, Alaska [Francis, 1976], Norway [Griffin, 1973], etc. In all these cases the presence of amph-peridotite was related either to metasomatic reactions involving deep-seated H_2O and alkali-rich fluids or to crystallization from impregnating liquids of alkali basalt composition.

The Zabargad amph-peridotites tend to be enriched relative to the sp-lherzolites in K, LREE, and, in one case where traces of apatite are present (Z-206), in P. The presence of apatite is not "per se" incompatible with an upper mantle origin since it appears to be stable at mantle's pressure and temperature [Beswick and Carmichael, 1968, Watson, 1980] and has been observed in sp-lherzolite xenoliths [Frey and Green, 1974] and in St. Paul amph-peridotite [Roden et al., 1984].

The LREE enrichment of the Zabargad amph-peridotites, which reaches a maximum in apatite-bearing sample Z-206 (Figure 14), is similar to that observed in other amph-peridotites of mantle origin, particularly those from St. Paul Rocks [Frey, 1970; Roden et al., 1984]. The amph-peridotites show La-Sm-Lu fractionations which are not compatible with melting products and cannot be explained solely in terms of crystal chemistry, i.e., fractionation according to REE ionic radii and available sites in mineral solid phases. These fractionations are probably related to the geochemical behavior of REE in the presence of a fluid phase, i.e., degree of basicity, capability of complexing, etc. Thus the REE composition of the amph-peridotites must result from

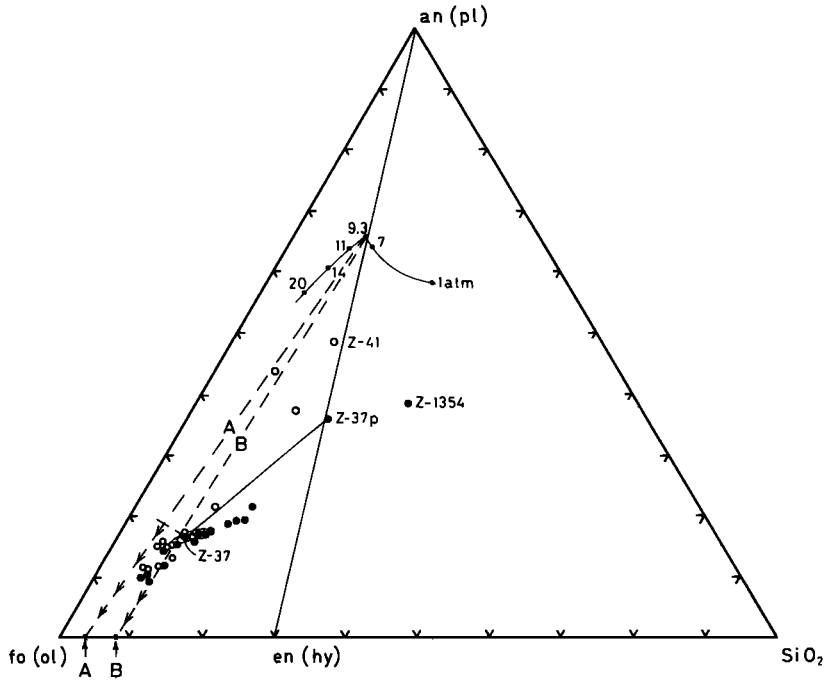

Fig. 20. Projection from the di apex onto the an-fo-q plane of the simplified tholeiitic basalt tetrahedron [Presnall et al., 1979, Figure 9]. Composition of initial melting liquids at different P total (numbers on the solid line) according to Presnall et al. [1979] are compared with the normative ol (fo + fa) - pl (an + ab) - q (SiO_2) composition of the studied rocks. Symbols are as in Figure 19. The dashed lines A and B join the composition of liquids produced at the cusp with the modal composition of peridotitic residue at the end of the peritectic melting event. The two trends A and B describe qualitatively the path followed by the residue starting from parental undepleted sp-peridotite assemblages.

"metasomatism", i.e., "a solid state transformation, with material transfer through a vapor or fluid phase" [Bailey, 1982]. The main metasomatic fluids that we need to consider are H_2O and CO_2.

Effects of Contamination by H_2O

The REE distribution between H_2O vapor and solid phases is strongly influenced by pressure: REE tend to be preferentially stabilized in the H_2O vapor as pressure increases. Experimental data on the partitioning of Sm between H_2O and diopside indicate an increase of stabilization of Sm in the fluid by a factor of 3×10^3 in the pressure range 5 to 30 kbar [Mysen, 1979, 1983]. Experimental data between other solid phases and H_2O vapor within the same pressure range [Mysen, 1979] and at lower pressures [Cullers et al., 1973; Zielinski and Frey, 1974], combined with crystal/crystal REE partitionings [Ottonello, 1980, 1981, and references therein], allow estimates of REE bulk solid/H_2O vapor distribution factors for peridotite assemblages at various pressures (Figure 23). These calculations cannot be extended to derive H_2O vapor/melt distribution factors at H_2O saturation, in as much as the bulk peridotite/melt distribution for these elements is a complex function of the degree of melting. The decrease in the REE H_2O/melt partition values with increasing pressure is due to the network-modifying effect of H_2O on the structure of the silicate liquid [Flynn and Burnham, 1978]. (According to the water-magma mixing model of Burnham [1975], the breakdown of polymer chains by substitution of hydroxyls with bridging oxygens results in an increase of available sites for REE in silicate melt. The increase of stabilization of high field strength ions with the decrease of polymerization [Hess, 1971; Watson, 1976; Ryeson and Hess, 1978] is also a general result of the application of polymer theory to silicate liquids [Toop and Samis, 1962a, b; Masson, 1965; Hess, 1971].)

In terms of solution chemistry, the equilibrium distribution of REE between vapor phase and silicate melt can be described by

$$REE^{3+}_{(v)} + 3(OH)_{(m)} = REE(OH)_{3(m)} \qquad (2)$$

The mass action effect suggests that the stabilization of trivalent REE in the melt increases with the third power of hydroxyl molality. According to calculations of H_2O solution in silicate melts on equimolal basis the hydroxyl activity is insensitive to composition effects [Burnham, 1975]. The third power of hydroxyl equimolal solubility, derived from the experimental equimolal solubility curve [Burnham, 1975] through application of the relation 7 of Flynn and Burnham [1978], varies linearly with pressure as follows:

$$X_{OH(m)}{}^3 \sim 0.00258 \cdot P\,(kbar) - 0.00074 \qquad (3)$$

The following expression is obtained at a given pressure, substituting activities for concentrations which roughly accounts for the pressure effect on the REE partitioning between H_2O vapor and melt:

$$K^{H_2O/melt}_{REE} = \frac{Const\ (P,T,X)}{K_{(1)} \times [0.00258 \cdot P(kbar) - 0.00074]} \qquad (4)$$

where the constant term accounts for nonideal behavior. Experimental runs [Flynn and Burnham, 1978] indicate that

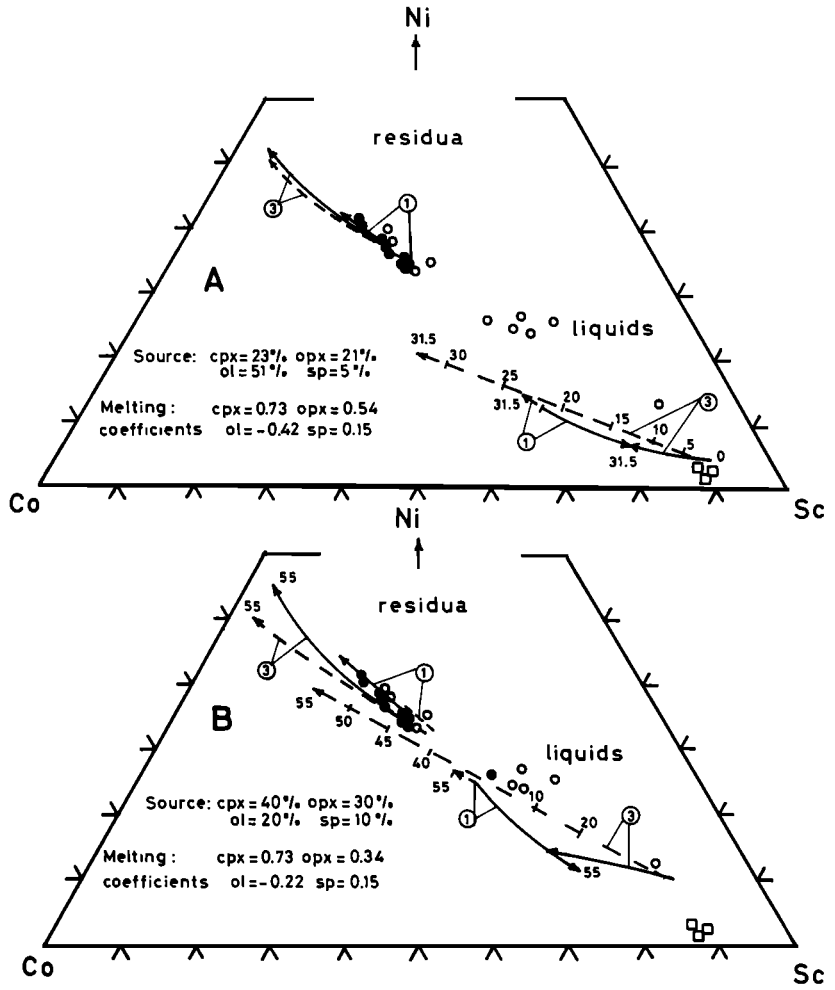

Fig. 21. Sc-Co-Ni fractionation trends in Zabargad peridotites (circles) and basalt dikes (squares) under two different sets of conditions. Values are normalized to Sc-Co-Ni contents in Z-37 protogranular sp-lherzolite (Table 15). Open circles are pl-peridotites; solid circles are sp-lherzolites. The modeled fractionation trends 1 and 3 were obtained with the partition coefficients sets 1 and 3 of Ottonello et al. [1984a] and are appropriate for T=1200° and T=1350°C respectively. Numerals on the trends refer to the percentage of partial melting. Dashed lines refer to fractional melting; solid lines to equilibrium melting.

the solubility constant K(1) is different for the different REE at the same pressure. Moreover, the bias introduced assuming independence of the Const/K(1) term from pressure is less significant than the variation introduced by the presence of other anionic ligands. The ruled field of REE distribution values for the H_2O vapor/sp-peridotite equilibrium at Ptot= 5 and 10 kbar is compared in Figure 23 with the H_2O vapor/melt REE distribution trends at the same pressures. We note that (1) pressure has an inverse effect on the H_2O vapor/melt and H_2O vapor/spinel peridotite REE equilibria, and (2) Eu is stabilized preferentially in the H_2O vapor in equilibrium with a silicate liquid relative to other REE, while no Eu anomaly can be derived from the existing H_2O vapor/solid experimental data. (The Eu anomaly could be due to the formation of complexes of the type Eu $(OH)_2$ in the liquid, whose stabilization depends on the second power of OH activity (and not on the third power as for other REE).)

H_2O-rich fluids rising from deeper mantle levels or released by upward intruding melts tend to be oversaturated in REE relative to the country rock due to the decrease of solubility during decompression and to the pressure gradient effect on the REE stabilization in the vapor phase. The degree of oversaturation depends on poorly known parameters, as presence of anionic ligands other than OH [Flynn and Burnham, 1978; Balashov and Krigman, 1975], rate of ascent, and equilibration rate. In any case, the permeation by the fluid of fracture systems will result in deposition of excess metals present in the fluid. (As an example, the Ce content in a H_2O vapor which equilibrated with country rock peridotite at Ptot = 10 kbar is about 300 times greater than the equilibrium content at Ptot = 5 kbar if the Ce content of the country rock is constant.)

Figure 23 shows A, the REE compositions of H_2O vapor in equilibrium with peridotite (chondritic REE composition) at Ptot = 10 kbar, T=1100°C (dashed area); B, the REE composition of H_2O vapor in equilibrium with incipient melting liquids (F = 1% at Ptot = 9 kbar, based on the melting model, and on relation 3 (solid line). The net result of continuous permeation by H_2O-rich solutions along fracture systems will be either a composition intermediate between sp-lherzolites and composition A if the fluids last equilibrated with peridotite deeper in the mantle or a composition intermediate between sp-lherzolites and trend B if the fluids were released at the beginning of a melting event localized at the cusp. Both compositions (particularly, in the second case, the existence of a Eu anomaly) are compatible with the

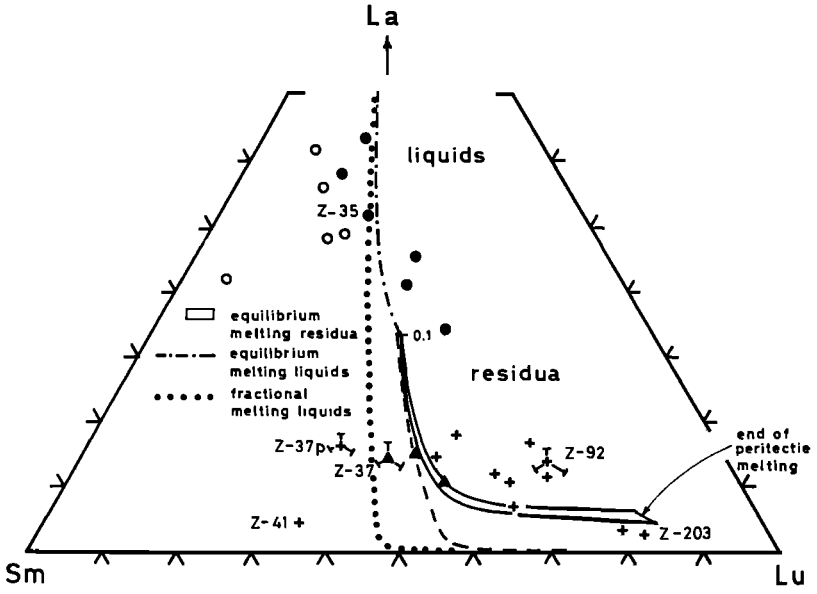

Fig. 22. La-Sm-Lu fractionations in Zabargad peridotites and basalt dikes. Triangles, sp-lherzolites. Crosses, pl-peridotites. Solid circles, amph-peridotites. Open circles, basalt dikes (unpublished data). Values are normalized to chondrites. The fractionation trends of the model were obtained adopting the set 1 of partition coefficients proposed by Frey et al. [1978] modified for the presence of spinel as accessory phase [Ottonello et al., 1984a]. The area on the equilibrium melting trend for residue includes uncertainty due to variability in the modal composition of the source and of variable melting proportions [Ottonello et al., 1984a].

Zabargad amph-peridotites, except for sample Z-206 which has a maximum enrichment factor at the Nd level and a marked negative Eu anomaly. Z-206 has, however, an anomalous P_2O_5 content (Table 12); thus REE may be present in this sample as phosphate complexes. We are not aware of experimental data on the REE stabilization in P_2O_5 rich fluids; however, we note that the REE fractionation in Z-206 mimics the apatite/liquid fractionation imposed on the REE by this mineral [Nagasawa, 1970].

Effects of Contamination by CO_2

The direct entrapment of CO_2, compatible with measured CO_2 contents in amph-peridotites, is not sufficient to explain their contamination with LREE. Experimental data on REE equilibria between CO_2-rich vapor phase and silicate melt [Wendlandt and Harrison, 1979] suggest that the pressure/stabilization gradient is similar to that calculated for H_2O vapor/melt REE equilibria (Figure 23). Moreover, the REE pressure/stabilization gradient in CO_2 vapor varies discontinuously through the REE series, being minimal for Sm and increasing toward LREE and HREE at low pressure [Wendlandt and Harrison, 1979]. The different stabilization for each single REE in CO_2 vapor, and the inverse pressure/stabilization gradient, are compatible with the formation of carbonate complexes in the vapor phase [Weale, 1967; Balashov and Kriegman, 1975].

Experiments on the partitioning of Sm between diopside and a vapor phase made of variable proportions of H_2O and CO_2 [Mysen, 1983] indicate that if the molar proportion of CO_2 in the vapor phase is increased, the vapor/diopside distribution value for Sm decreases. Moreover, if the total pressure is increased, the CO_2 vapor/diopside distribution factor increases, as observed also in H_2O/diopside equilibria.

The vapor/sp-peridotite REE distribution trend shown in Figure 23 was calculated by Mysen [1983] for T = 100°C, Ptot = 20 kbar, and molar proportion of CO_2 in the vapor phase varying from $X_{CO_2} = 0$ (line G in Figure 23) and $X_{CO_2} = 1$ (line H in Figure 23). The differential LREE/HREE fractionation between calculated fields A and G-H depends upon the choice of different solid/solid partition values for REE in the sp-peridotite assemblage. According to experimental data, therefore, the presence of CO_2 in the fluid phase does not significantly modify the contamination model suggested for H_2O-rich fluids.

We conclude that the Zabargad amph-peridotites probably originated from reactions of metasomatic H_2O-alkali-LREE-rich fluids with sp-lherzolites in the upper mantle. Reactions ranging from

$$H_2O\text{-fluid} + opx + cpx + Al\text{-spinel} \rightarrow amph + Cr\text{-spinel}$$

to

$$H_2O\text{-fluid} + cpx + spinel \rightarrow amph$$

which have been suggested to explain mantle-derived amph-peridotites from Casson [Conquere, 1971], Grand Canyon [Best, 1974], and Nunivak Island [Francis, 1976], might have operated also in the case of the Zabargad amph-peridotites. These reactions are consistent with the scarcity or absence of modal cpx and Al-spinel in amph-peridotites such as Z-206, where the green-brown Al-spinel is replaced by small opaque chromite and magnetite grains scattered within and around the amphibole crystals.

The origin of the metasomatic fluids is not clear at this stage of our study; they might have been released (1) from melts due to loss of solubility during decompression of the ascending mantle body, or, more probably, (2) from "degassing" of deeper levels of the mantle [Lloyd and Bailey, 1975; Boettcher et al., 1979; Bailey, 1982], which might include separation from a volatile- and alkali-rich carbonatitic melt [Wass and Rogers, 1980].

St. Paul (Atlantic) and Kiama (Australia) amph-peridotites have been suggested as possible source material for alkali basalt melts [Roden et al., 1984; Wass and Rogers, 1980].

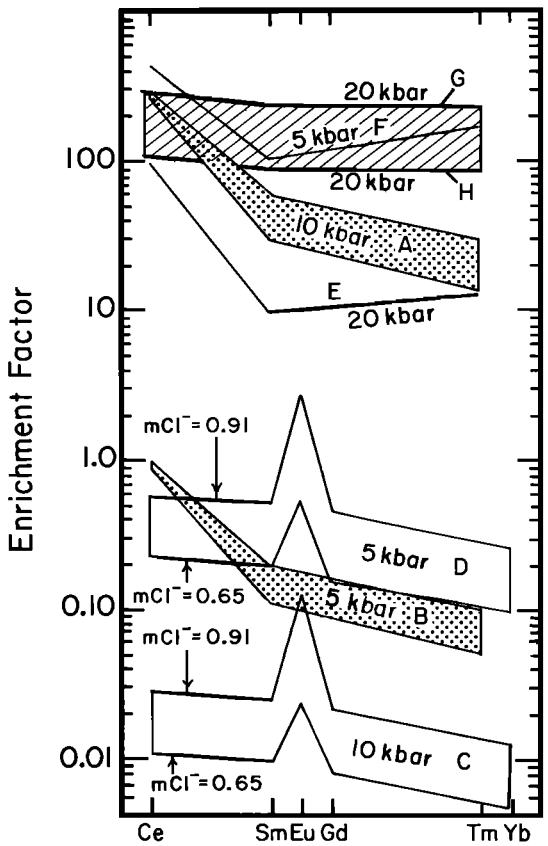

Fig. 23. Effects of pressure conditions on H_2O/peridotite; H_2O/melt; CO_2/melt and vapor (H_2O + CO_2)/peridotite REE equilibria. C and D are based on experimental data and application of relation 3 in the assumption of negligible effect of temperature. Trends E and F: data from Wendlandt and Harrison [1979]; A and B calculated from data by Mysen [1979] at high-P conditions and measured partitioning in residual sp-peridotite assemblages [Ottonello, 1980, 1981]. G and H calculated by Mysen [1983] at increasing X^{CO_2} molarity in the vapor phase from $X^{CO_2} = 0$ (G) to $X^{CO_2} = 1$ (H). A, C; $P_{tot} = 10$ kbar; B, D: $P_{tot} = 5$ kbar; A, B: $D^{H_2O/peridotite}_{REE}$; C, $D = D^{H_2O/melt}_{REE}$. E: $D^{CO_2/melt}_{REE}$, $P_{tot} = 20$ kbar; F: $D^{CO_2/melt}_{REE}$, $P_{tot} = 5$ kbar; G, H: $D^{vapor(H_2O+CO_2)/melt}$, $P_{tot} = 20$ kbar; T = 1100°C.

Similarly, in terms of major and RE elements, Zabargad amph-peridotites such as Z-206, with >10% modal hornblende and detectable amounts of modal apatite and phlogopite, can be a potential source of alkali basalt by small degrees of partial melting.

Concluding Remarks on the Origin of the Zabargad Peridotites

1. Textures, mineralogy, and mineral chemistry as well as major, REE, and transition element compositions of the Zabargad protogranular sp-lherzolites, all give concordant information. These rocks can be regarded as upper mantle material which equilibrated in the sp-lherzolite facies, that is, at pressures equivalent to at least 30 km beneath the surface. Some of these rocks can be regarded as residual after a small melting event, with the mass of the liquid not exceeding a few percent of the initial system. Some of the samples appear to be unaffected by the melting event and approach a parental mantle composition.

2. The Zabargad pl-peridotites can be considered either as mixed portions of residuum and a small melt fraction, which was not removed after a minor, localized peritectic melting event, or as resulting from incorporation of an exotic melt fraction through localized injections into the ascending lherzolite body. Though both hypotheses are consistent with trace element data, the second hypothesis agrees better with field and petrographic data. The exotic melt probably derived from a deeper source in the mantle, similar in composition to the sp-lherzolites. The Zabargad pl-peridotites could be an example of mantle material with a small trapped melt fraction, related to the low-velocity zone inferred to be present in the upper mantle beneath oceanic and continental rifts. The basaltic dikes crossing the Zabargad lherzolites probably represent more recent, shallower events of melt injection which affected the rising mantle body close to the surface.

3. The Zabargad amph-peridotites show evidence of metasomatic contamination by H2O-rich fluids which were probably injected locally into the ascending lherzolite body. The metasomatic fluid could either be derived from within the same mantle by processes of autometasomatism or be related to degassing of alkali-rich or even carbonatitic melts. As suggested by Roden et al. [1984] for St. Paul amph-peridotites, the Zabargad amph-peridotites could be a potential source of alkali basalt magma by small degrees of partial melting. The metasomatic processes which affected the Zabargad lherzolite are perhaps related to the extensive mantle metasomatism thought to affect incipient rift zones [Bailey, 1978].

4. The field distribution of sp-lherzolites, pl-peridotites, and amph-peridotites suggest small (meter) scale dishomogeneity in the upper mantle source for the Zabargad ultramafic body. This is illustrated by a section about 20 m thick sampled in detail in the Central Peridotite Body. This section is made mainly of sp-lherzolites but includes pl-peridotite and amph-peridotite zones.

5. Precambrian-Paleozoic ophiolitic complexes have been identified in circum-Red Sea areas, including the Egyptian Eastern Desert region [Dixon, 1979; Shackleton et al., 1980]. One possibility to be considered is that the Zabargad peridotites are equivalent in age and origin to ultramafic massifs which are exposed in the Eastern Desert region of Egypt, that is, in the area of the African continent adjacent to the Red Sea coast at latitudes similar to that of Zabargad (Figure 24). Of the ultramafic complexes exposed in the Eastern Desert Region, two distinct types have been identified [Dixon, 1979]: those representing lower crustal layered complexes (for example, the Dahanib complex) and those which were emplaced tectonically and have some features similar to those of ophiolites. The former have no similarity to the Zabargad ultramafics which are clearly of mantle derivation and were emplaced tectonically. The latter, such as the Zeidun-Massam and the Um Seleimat complexes, were interpreted by Dixon [1979] to be former mantle-crust fragments with some oceanic affinity, probably representing an ancient marginal basin-island arc environment of late Precambrian-early Paleozoic age. The possibility that the Zabargad peridotites represent also a Precambrian-Paleozoic complex similar to those exposed on the Egyptian mainland and elsewhere in circum-Red Sea areas has been explored.

A comparison between the Zabargad and the Eastern Desert ultramafic complexes indicates that (1) the Zabargad ultramafics are not serpentinized and the mainland ultramafics are very strongly serpentinized, (2) the Zabargad ultramafics are mainly lherzolitic and the mainland ultramafics are harzburgites and dunites, and (3) mineral chemistry of the Zabargad and mainland ultramafics (exemplified by the Zeidum-Massar complex studied by Dixon) are quite different. Fo content of olivines lies within the 87-90% range in the Zabargad rocks but within the 84-86% range in the Zeidum-Masser rocks (Figure 5). The Al and En-Fs-Di-Hd content of opx (Figures

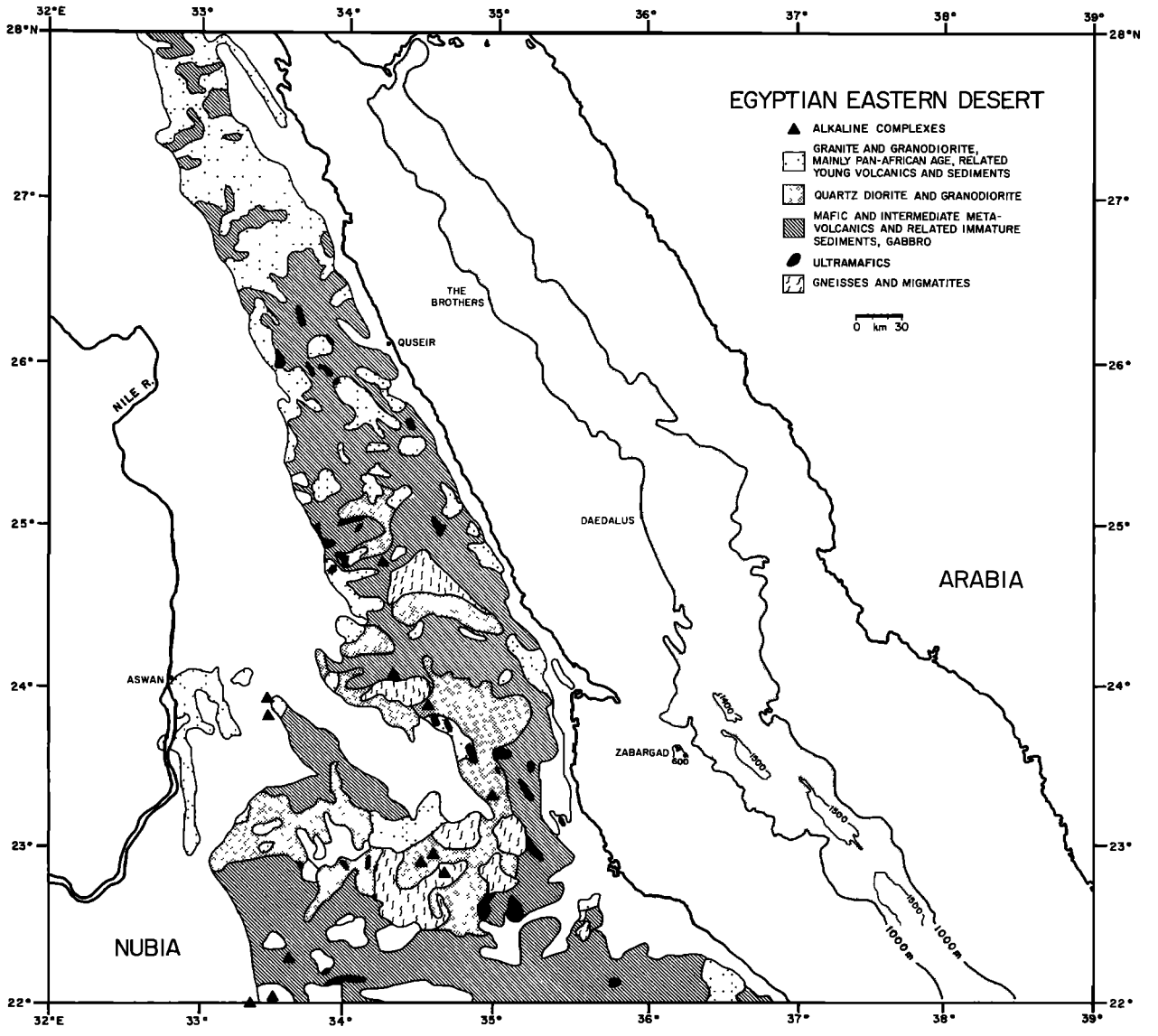

Fig. 24. Location of the Zabargad ultramafic massif relative to the main structural features of the central and northern Red Sea. Note the change in orientation of the Red Sea axis from a NW-SE to a roughly N-S direction in a segment extending from about the latitude of Zabargad to about 25°N.

6 and 7) and the Mg-Cr-Fe^{2+}-Al content of spinel are also quite different. In fact, some of the mineral chemistry data for the Zeidum-Massar Eastern Desert complex suggest affinities with stratified basic complexes of lower crustal origin rather than with mantle-derived tectonites.

We conclude that the Zabargad peridotites have no similarity with the Precambrian-Paleozoic ultramafic complexes exposed in Egypt and in other circum-Red Sea areas, and we suggest that they have a different origin.

6. Field evidence is compatible with the Zabargad peridotites having been emplaced in post-Mesozoic times, i.e., in connection with the formation of the Red Sea rift [Bonatti, et al., 1981, 1983]. Direct, absolute age constraints are not yet available. However, the relatively young age of emplacement of the Zabargad ultramafics is supported by their exceptional freshness and lack of serpentinization. The three distinct ultramafic bodies mapped at Zabargad are probably surface exposures of a single mantle protrusion, wider in diameter than the island, as suggested by the broad positive gravity anomaly centered on the island [Allan, 1970; Styles and Gerdes, 1983]. The absence of serpentinization and the lack of equilibration in the pl-peridotite stability field suggest a relatively rapid ascent of the ultramafic body through the upper mantle and crust.

7. Two different mechanisms probably caused the emplacement of the Zabargad mantle body. The deeper stages in the ascent through the upper mantle of the Zabargad peridotite body may be due to asthenospheric upwelling in a thermally anomalous rift zone, and may be related to the opening of the Red Sea rift. The shallower stages of ascent at crustal levels, which resulted in emersion of the island of Zabargad, are probably related to the complex tectonic framework of the central Red Sea. Zabargad is located along an ancient but rejuvinated tectonic alignment transversal to the Red Sea axis [Garson and Krs, 1976; Bonatti et al., 1981, 1983, 1984; Bonatti, 1985] which we have called the Zabargad Fracture Zone. This fracture zone strikes about N-S, i.e., from 000° to 020°N. The positive gravity anomaly centered on Zabargad is elongated in a roughly N-S direction [Styles and Gerdes, 1983], suggesting that the mantle body

exposed on the island extends at shallow levels in the same direction, i.e., parallel to the fracture zone. The direction of the Red Sea axis changes at this latitude by about 50° and becomes roughly parallel to the suggested fracture zone from about 23°N to 25°N (Figure 24). Localized compressional or tensional stresses can develop along fracture zones [Bonatti, 1978; Karson et al., 1983], even where little or no transform motions occur. Tectonic uplift may result from such compressional events. Moreover, the Zabargad Fracture Zone is located close to the tip of the northward propagating oceanic rift at the axis of the Red Sea [Bonatti et al., 1984; Bonatti, 1985]. The impact of the propagating rift against the fracture zone may also cause zones of compression. In addition, the surface exposure of the Zabargad mantle body may have been favored by the fact that the crust of this region of the Red Sea is attenuated in thickness.

A structural situation similar to that described here has been reported for the Iberian margin of the Atlantic [Boillot et al., 1980] and for the SW Australian margin of the Indian Ocean [Nicholls et al., 1981]. In both cases, mantle-derived ultramafic bodies are exposed on the ocean floor close to the boundary between oceanic and attenuated continental crust. A Mesozoic example of emplacement of mantle lherzolites in thinned continental crust, similar to Zabargad, has been described in the northern Pyrenees [Vielzeuf and Kornprobst, 1984].

8. Textures, mineralogy, mineral chemistry, and elemental geochemistry of the Zabargad peridotites suggest some similarity with a number of mantle-derived ultramafic bodies samples in the ocean basins, such as the Owen Fracture Zone lherzolites [Bonatti and Hamlyn, 1978; Hamlyn and Bonatti, 1980] and the St. Paul ultramafics [Melson et al., 1972; Roden et al., 1984]. However, oceanic ultramafics of mantle derivation tend generally to be more depleted than the Zabargad sp-lherzolites. Given that the Zabargad lherzolites were emplaced in a pre-oceanic rift, they may be said to represent oceanic mantle before extraction of the basaltic oceanic crust.

Acknowledgments. Research supported by National Science Foundation grant OCE 83-15933, Office of Naval Research contract N000-80-C-0098/T, and the Italian CNR (Gruppo Informale Africa). Trace element analyses have been performed at the Pierre Sue Laboratory (CEA Saclay, Paris). We are indebted to M. Treuil and the "Groupe des Sciences de la Terre" for their kind hospitality. J.L. Joron helped one of us (G.O.) in the radioanalytical and instrumental procedures. We are grateful to R. Gelmini, G. Marinelli, A. Olshki, and M. Taviani for help in the field work. Constructive reviews by H. Dick, F. Frey, D. Walker, and A. Kudo greatly improved this paper. We thank D. Breger for technical assistance throughout this work and we are indebted to W.B.F. Ryan for his gracious help. Lamont-Doherty Geological Observatory of Columbia University contribution 3904.

References

Allan, T. D., Magnetic and gravity fields over the Red Sea, Philos. Trans. R. Soc. London, Ser. A, 267, 153-180, 1970.

Arai, S., and T. Fujii, Petrology of ultramafic rocks from site 395, Initial Rep. Deep Sea Drill. Proj., 45, 587-594, 1979.

Bailey, D. K., Continental rifting and mantle degassing, in Petrology and Geochemistry of Continental Rifts, edited by E. R. Neumann and I. B. Ramberg, pp. 1-13, D. Reidel, Hingham, Mass., 1978.

Bailey, D. K., Mantle metasomatism-continuing chemical change within the earth, Nature, 296, 525-530, 1982.

Balashov, Yu. A., and L. D. Krigman, The effects of alkalinity and volatiles on rare earth separation in magmatic systems, Geochem. Int., 12, 165-170, 1975.

Best, M. G., Mantle-derived amphibole within inclusions in alkalic basaltic lavas, J. Geophys. Res., 79, 2107-2113, 1974.

Bestwick, A. E., and J. G. E. Carmichael, Constraints on mantle source com-positions imposed by phosphorous and the rare earth elements,Contrib. Mineral. Petrol., 67, 317-330,1968.

Boetcher, A. L., J. R. O'Neil, K. E. Windom, D. C. Steward, and H. G. Wilshire, Metasomatism in the upper mantle and the genesis of kimberlites and alkkkali basalts, in The Mantle Sample: Inclusions in kimberlites and Other Volcanics, edited by F. R. Boyd and H. O. A. Meyer, pp. 173-182, AGU, Washington, D. C., 1979.

Boillot, G., S. Grimand, A. Mauffret, D. Mougenot, J. Kornprobst, G. Mergoil, and G. Torrent, Ocean-continent boundary off the Iberian margin: A serpentinite diapir west of the Galicia Bank, Earth Planet. Sci. Lett., 48, 23-24, 1980.

Bonatti, E., Vertical tectonism in oceanic fracture zones, Earth Planet. Sci. Lett., 37, 369-379, 1978.

Bonatti, E., Punctiform initiation of seafloor spreading in the Red Sea during transition from a continental to an oceanic rift, Nature, 316, 33-37, 1985.

Bonatti, E., and P. R. Hamlyn, Mantle uplifted block in the western Indian Ocean, Science, 201, 249-251, 1978.

Bonatti, E., and P. R. Hamlyn, Oceanic ultramafic rocks, in The Sea, vol. 7, The Oceanic Lithosphere, pp. 241-283, John Wiley, New York, 1981.

Bonatti, E., and J. Honnorez, Sections of the earth's crust in the equatorial Atlantic, J. Geophys. Res, 81, 4104-4116, 1976.

Bonatti, E., P. R. Hamlyn, and G. Ottonello. The upper mantle beneath a young oceanic rift: Peridotites from the island of Zabargad (Red Sea), Geology, 9, 474-479, 1981.

Bonatti, E., R. Clocchiatti, P. Colantoni, R. Gelmini, G. Marinelli, G. Ottonello, R. Santacroce, M. Taviani, A. A. Abdel-Mequid, H. S. Assaf, and M. A. El Tahir, Zabargad (St. John) Island: An uplifted fragment of sub-Red Sea lithosphere, J. Geol. Soc. London, 140, 677-690, 1983.

Bonatti, E., P. Colantoni, B. Della Vedova, and M. Taviani, Geology of the Red Sea transitional region (22°N-25°N), Oceanol. Acta, 7, 385-398, 1984.

Boudier, F., Structure and petrology of the Lanzo peridotite massif (Piedmont Alps), Geol. Soc. Am. Bull., 89, 1574-1591, 1978.

Boyd, F. R., Hydrothermal investigations of amphiboles, in Researches in Geochemistry, vol. I, edited by H. Abelson, pp. 377-396, J. Wiley and Sons, New York, 1959.

Burnham, C. W., Water and magmas: A mixing model, Geochim. Cosmochim. Acta, 39, 1077-1084, 1975.

Burns, R. G. Mineral Applications of Crystal Field Theory, Cambridge Univ. Press, Cambridge, England, 250 p., 1970.

Carter, J. L., Mineralogy and chemistry of the earth's upper mantle based on the partial fusion-partial crystallization model, Geol. Soc. Am. Bull., 81, 2021-2034, 1970.

Clocchiatti, R., D. Massare, and C. Jehanno, Origin hydrothermale des olivines gemmes de l'ile de Zabargad (St. John), Mer Rouge, par l'etude de leurs inclusions, Bull. Mineral., 104, 354-360, 1981.

Conquere, F., La lherzolite a amphibole du gisement de Cassou (Ariege, France), Contrib. Mineral. Petrol., 30, 296-313, 1971.

Cullers, R. L., L. G. Medaris, and L. A. Haskin, Experimental study of the distribution of rare earths as trace elements among silicate minerals and liquid and water, Geochim. Cosmochim. Acta, 37, 1499-1512, 1973.

Dick, H. J. B., Partial melting in the Josephine peridotite, I, The effect on mineral composition and its consequence for geobarometry and geothermometry, Am. J. Sci., 277, 801-832, 1977.

Dick, H. J. B., and T. Bullen, Chromian spinel as a petrogenetic indicator in abyssal and alpine-type peridotites and spatially associated lavas, Contrib. Mineral. Petrol., 86, 54-76, 1984.

Dick, H. J. B., and R. L. Fisher, Mineralogic studies of the residues of mantle melting: Abyssal and alpine-type peridotites, in Kimberlites: The Mantle and Crust-Mantle Relationships, edited by J. Kornprobst, pp. 295-308, Elsevier, Amsterdam, 1984.

Dickey, V. S., Partial fusion products in Alpine-type peridotites: Serrania de la Ronda and other examples, Mineral. Soc. Am. Spec. Pap., 3, 33-49, 1970.

Dixon, T. H., The evolution of the continental crust in the last Precambrian Egyptian Shield, Ph.D. thesis, 231 pp., Univ. of Calif., San Diego, La Jolla, 1979.

Dostal, J., and G. K. Muecke, Trace element geochemistry of the peridotite-gabbro-basalt suite from DSDP leg 37, Earth Planet Sci. Lett., 90, 915-922, 1977.

El Shazly, E. M., and G. S. Saleeb, Scapolite-cancrinite mineral association in St. John's Island, Egypt, Int. Geol. Congr., 24th, 192-199, 1972.

Flynn, R. T., and C. W. Burnham, An experimental determination of rare earth partition coefficients between a chloride containing vapor phase and silicate melts, Geochim. Cosmochim. Acta, 42, 685-701, 1978.

Francis, D. M., The origin of amphibole in lherzolite xenoliths from Nunivak Island, Alaska, J. Petrol., 17, 357-378, 1976.

Franzini, M., L. Leoni, and M. Saitta, Revisione di una metodologia analitica per fluorescenza-X, basata sulla correzione completa degli effetti di matrice, Rend. Soc. Ital. Mineral. Petrol, 31(2), 365-378, 1975.

Frey, F. A., Rare earth abundances in a high temperature peridotite intrusion, Geochim. Cosmochim. Acta, 33, 1429-1447, 1969.

Frey, F. A., Rare earth and potassium abundances in St. Paul's rocks, Earth Planet. Sci. Lett., 7, 351-360, 1970.

Frey, F. A., and D. M. Green, The mineralogy, geochemistry and origin in lherzolite inclusions in Victorian basanites, Geochim. Cosmochim. Acta, 38, 1023-1059, 1974.

Frey, F. A., L. A. Haskin, and M. A. Haskin, Rare-earth abundances in some ultramafic rocks, J. Geophys. Res., 76, 2057-2070, 1971.

Frey, F. A., D. M. Green, and S. D. Roy, Integrated models of basalts petro-genesis: A study of quartz tholeiites to olivine melilites from south-eastern Australia utilizing geochemical and experimental petrological data, J. Petrol., 19, 463-513, 1978.

Garson, M. S., and M. Krs, Geophysical and geological evidence of the relationships of the Red Sea transverse tectonics to ancient fractures, Geol. Soc. Am. Bull., 87, 169-181, 1976.

Gilbert, M. C., R. T. Helz, R. K. Popp, and F. S. Spear, Experimental studies of amphibole stability, Rev. Mineral., 9B, 229-346, 1982.

Green, D. H., The petrogenesis of the high-temperature peridotite intrusion in the Lizard area, Cornwall, J. Petrol., 5, 134-188, 1964.

Green, D. H., and W. Hibberson, The instability of plagioclase in peridotite at high pressure, Lithos, 3, 209-221, 1970.

Green, D. H., and A. E. Ringwood, The stability fields of aluminous pyroxene peridotite and garnet peridotite and their relevance to upper mantle structure, Earth Planet. Sci. Lett., 3, 151-160, 1967.

Green, D. H., A. E. Ringwood, N. G. Ware, and W. O. Hibberson, Experimental petrology and petrogenesis of Apollo 14 basalts, Proc. Lunar Sci. Conf., 3rd, 197-206, 1972.

Griffin, W. L., Lherzolite nodules from the Fen alkaline complex, Norway, Contrib. Mineral. Petrol., 38, 135-146, 1973.

Hamlyn, P. R., and E. Bonatti, Petrology of mantle-derived ultramafics from the Owen F.Z., northwest Indian Ocean: Implications for the nature of the oceanic upper mantle, Earth Planet. Sci. Lett., 48, 63-79, 1980.

Harte, B., Rock nomenclature with particular relation to deformation and recrystallizjation textures in olivine-bearing xenoliths, J. Geol., 85, 279-288, 1977.

Hess, P. E., Polymer model of silicate melts, Geochim. Cosmochim. Acta, 35, 289-306, 1971.

Irvine, T. N., Chromian spinel as a petrogenetic indicator, Can. J. Earth Sci., 4, 71-103, 1967.

Jacobsen, S. B., J. E. Quick, and G. J. Wasserburg, A Nd and Sr isotopic study of the Trinity peridotite: Implications for mantle evolution, Earth Planet. Sci. Lett., 68, 361-378,1984.

Jaques, A. L., and D. H. Green, Anhydrous melting of peridotite at 0-15 kb pressure and the genesis of tholeiitic basalts, Contrib. Mineral. Petrol., 73, 287-310, 1980.

Joron, J. L., and G. Ottonello, Radiochemical neutron activation analysis of rare earth elements in peridotitic rocks, J. Radioanal. Nuclear Chem., 88-2, 259-272, 1985.

Karson, J. A., D. L. Elthon, and S. E. DeLong, Ultramafic Intrusions in the Lewis Hills Massif, Bay of Islands Ophiolite Complex, Newfoundland: Implications for igneous processes at oceanic fracture zones, Geol. Soc. Am. Bull., 94, 15-29, 1983.

Kay, R., N. Hubbard and P. Gast, Chemical characteristics and origin of oceanic ridge volcanic rocks, J. Geophys. Res., 75, 1585, 1970.

Kornprobst, J., D. Ohnestetter, and M. Ohnestetter, Na and Cr contents in clinopyroxenes from peridotites: A possible discriminant between "sub-continental" and "sub-oceanic" mantle, Earth Planet. Sci. Lett., 53, 241-254, 1981.

Kushiro, I., Y. Syono, and S. Akimoto, Stability of phlogopite at high pressures and possible presence of phlogopite in the earth's upper mantle, Earth Planet. Sci. Lett., 3, 197-203, 1967.

Langmuir, C. H., J. F. Bender, A. E. Bence, G. N. Hanson, and G. R. Taylor, Petrogenesis of basalts from the FAMOUS area: Mid-Atlantic Ridge, Earth Planet Sci. Lett., 36, 133-156, 1977.

Leake, B. E. A catalog of analyzed calciferous and subcalciferous amphiboles together with their nomenclature and associated minerals, Geol. Soc. Am., Spec. Pap. 98, 210p., 1968.

Leoni, L., and M. Saitta, X-rays fluorescence analysis of 29 trace elements in rock and mineral standards, Rend. Soc. Ital. Mineral Petrol., 32(2), 497-510, 1976.

Lloyd, F.E., and D.K. Bailey, Light element metasomatism of the continental mantle: The evidence and the consequences, Phys. Chem. Earth., 9, 389-416, 1975.

Loubet, M., M. Shimizu, and C. J. Allegre, Rare earth elements in alpine peridotites, Contrib. Mineral. Petrol., 53, 1-12, 1975.

Maaloe, S., and K. Aoli, The major element composition of the upper mantle estimated from the composition of lherzolites, Contrib. Mineral. Petrol., 63, 161-173, 1977.

Masson, C. R. , An approach to the problem of ionic distribution in liquid silicates, Proc. R. Soc. London, Ser. A, 287, 201-221, 1965.

Masuda, A., and H. Jibiki, Rare earth patterns of Mid-Atlantic Ridge gabbros: Continental nature, Geochem. J., 7, 55-65, 1973.

Melson, W.G., E. Jarosewich, V.T. Bowen, and G. Thompson, St. Peter and St. Paul rocks: A high-

temperature, mantle-derived intrusion, Science, 155, 1532-1535, 1967.
Melson, W.G., S.R. Hart, and G. Thompson, St. Paul's rocks, equatorial Atlantic: Petrogenesis, radiometric ages and implications on sea floor spreading, Mem. Geol. Soc. Am., 132, 241-272, 1972.
Menzies, M., Rare earth geochemistry of fused ophiolitic and alpine lherzolites, I, Othrys, Lanzo and Troodos, Geochim. Cosmochim. Acta, 40, 645-656, 1976.
Menzies, M.A., and C. Allen, Plagioclase lherzolites-residual mantle relationships within the eastern Mediterranean ophiolites, Contrib. Mineral. Petrol., 45, 197-213, 1974.
Menzies, M., D. Blauchard, J. Brannon, and R. Korotev, Rare earth geochemistry of fused ophiolitic and alpine lherzolites, II, Beni Bouchera, Ronda and Lanzo, Contrib. Mineral. Petrol., 64, 53-74, 1977.
Mercier, J.C., and A. Nicolas, Textures and fabrics of upper mantle peridotites as illustrated by xenoliths from basalts, J. Petrol., 16, 654-687, 1975.
Michael, P.J., and E. Bonatti, Peridotite composition from the North Atlantic: Regional and tectonic variations and implications for partial melting, Earth Planet. Sci. Lett., 73, 91-104, 1985.
Moon, F.W., Preliminary geological report on St. John island (Red Sea), 36 p., Geol. Surv. of Egypt, Government Press, Cairo, 1923.
Mysen, B.O., Trace element partitioning between garnet peridotite minerals and water-rich vapor: Experimental data from 5 to 30 kbar, Am. Mineral., 64., 274-287, 1979.
Mysen, B.O., Rare earth element partitioning between (H_2O + CO_2) vapor and upper mantle minerals: Experimental data bearing on the conditions of formation of alkali basalt and kimberlite, Neues Jahrb. Mineral. Abh., 146, 41-65, 1983.
Nagasawa, H., Rare earth concentrations in zircons and apatites and their host dacites and granites, Earth Planet. Sci. Lett., 9, 359-364, 1970.
Nagasawa, H., H. Wakika, H. Higuchi, and N. Onuma, Rare earths in peridotite nodules: An explanation of the genetic relationship between basalt and peridotite nodules, Earth Planet. Sci. Lett., 5, 377-381, 1969.
Nicholls, I.A., J. Ferguson, H. Jones, G.P. Marks, and J.C. Mutter, Ultramafic blocks from the ocean floor southwest of Australia, Earth Planet. Sci. Lett., 56, 362-374, 1981.
Nicolas, A., and C. Dupuy, Origin of ophiolitic and oceanic lherzolites, Tectonophysics, 110, 177-178, 1984.
O'Hara, M.J., The bearing of phase equilibria studies in synthetic and natural systems in the origin and evolution of basic and ultrabasic systems on the origin and evolution of basic and ultrabasic rocks, Earth Sci. Rev., 4, 69-133, 1968.
O'Hara, M.J., and S.W. Richardson, and G. Wilson, Garnet-peridotite stability and occurrence in crust and mantle, Contrib. Mineral. Petrol., 32, 48-67, 1971.
Ottonello, G., Attivazione neutronica: Applicazione delle metodologie radionanalitiche e strumentali all'indagine geochimica, Rend. Soc. Ital. Mineral. Petrol., 35, 527-533, 1979.
Ottonello, G., Rare earth abundances and distribution in some spinel peridotite xenoliths from Assab (Ethiopia), Geochim. Cosmochim. Acta, 44, 1885-1901, 1980.
Ottonello, G., Alcuni aspetti della geochimica delle terre rare in rocce peridotitiche, tesi di perfezionamento in Scienze Geologiche, 85 p., Scuola Normale Superiore, Pisa.
Ottonello, G., G. B. Piccardo, and W. G. Ernst, Petrogenesis of some Ligurian peridotites, II, Rare earth chemistry, Geochim. Cosmochim. Acta, 43, 1273-1284, 1980a.
Ottonello, G., G. B. Piccardo, J. L. Joron, and M. Treuil, Nature of the deep crust and uppermost mantle under the Assab Region (Ethiopia): Inferences from petrology and geochemistry of mafic-ultramafic inclusions, Proceedings of the Symposium on the Evolution of the Afro-Arabian Rift System, Rome, Atti Accad. Lincei, 47, 4633-490, 1980b.
Ottonello, G., W.G. Ernst, and J. L. Joron, REE and transition elements geochemistry of peridotitic rocks, I Peridotites from the W. Alps, J. Petrol., 25, 343-372, 1984a.
Ottonello, G., G. B. Piccardo, and J.L. Joron, REE and transition elements geochemistry of peridotitic rocks, II Ligurian peridotites and associated basalts, J. Petrol., 25, 379-393, 1984b.
Philpotts, J.A., C.C. Schcnetzler, and H. H. Thomas, Petrogenetic implications of some new geochemical data on eclogitic and ultrabasic inclusions, Geochim. Cosmochim. Acta, 36, 1131-1166, 1972.
Pike, J. E. N., and E.C. Schwarzman, Classification of textures in ultramafic xenoliths, J. Geol., 85, 49-61, 1977.
Poldervaart, A., and H. H. Hess, Pyroxene in the crystallization of basaltic magma, J. Geol., 59, 472-489, 1951.
Presnall, D. C., J. R. Dixon, T. H. O'Donnell, and S.A. Dixon, Generation of midocean ridge tholeiites, J. Petrol., 20, 3-34, 1979.
Prinz, M., K. Keil, J. A. Green, A. M. Reid, E. Bonatti, and J. Honnorez, Mineralogy and petrology of some ultramafic and mafic dredge samples from the equatorial Mid-Atlantic Ridge and fracture zones, J. Geophys. Res., 81, 4087-4103, 1976.
Ridley, W. J. , and J. B. Dawson, Lithophile trace element data bearing on the origin of peridotite xenoliths, ankaramite and carbonatite from Lashaine volcano, N. Tanzania, Phys. Chem. Earth, 9, 545-559, 1975.
Ringwood, A. E., Chemical evolution of the terrestrial planets, Geochim. Cosmochim. Acta, 30, 41-104, 1966a.
Ringwood, A. E., The chemical composition and origin of the earth, in Advances in Earth Science, edited by P. Hurley, pp. 287-356, MIT Press, Cambridge, Mass., 1966b.
Ringwood, A. E., Composition and Petrology of the Earth's Mantle, McGraw-Hill, New York, 1975.
Ringwood, A. E., Origin of the Earth and Moon, Springer-Verlag, New York, 1979.
Robinson, P., F. S. Spear, J.C. Schumacher, J. Laird, C. Klein, B. W. Evans, and B. L. Doolan, Phase relations of metamorphic amphiboles: Natural occurrence and theory, Rev. Mineral., 9b, 1-211, 1982.
Roden, M., S. R. Hart, and F. A. Frey, REE and Sr, Nd and Pb isotopic geochemistry of St. Paul's rocks: The metamorphic and metasomatic development of an alkali basalt source, Contrib. Mineral. Petrol., 85, 376-390, 1984.
Ross, J. E., and L. H. Aller, The chemical compositon of the sun. Science, 191, 1223-1229, 1976.
Ryeson, F. J., and P. C. Hess, Implications of liquid distribution coefficients to mineral-liquid partitioning, Geochim. Cosmochim. Acta, 92, 921-932, 1978.
Schubert, C. E., Rare earth element distribution in equatorial Mid-Atlantic Ridge gabbros, Nature Phys. Sci., 237, 26-28, 1972.
Shackelton, R. N., A. C. Ries, R. H. Graham, and W. R. Fitches, Late Precambrian ophiolitic melange in the eastern desert of Egypt, Nature, 285, 472-474, 1980.
Shih, C., The rare earth geochemistry of oceanic igneous rocks, Ph.D. thesis, Columbia Univ., New York, 1972.
Shih, C., and P. Gast, Rare earths in abyssal tholeiites, gabbros and their mineral separates from Mid-Atlantic Ridge near 24°W, EOS Trans. AGU, 52, 376, 1971.
Shimizu, N., Geochemistry of ultramafic inclusions from Salt Lake Crater, Hawaii, and from southern African kimberlites, in Physics and Chemistry of the Earth, vol. 9, edited by T.J. Ahrens, pp. 655-669, Dawson, Duncan, Erlank, New York, 1975.

Sigurdsson, H., and J.G. Schilling, Spinels in Mid-Atlantic Ridge basalts: Chemistry and occurrence, Earth Planet. Sci. Lett., 29, 7-20, 1976.

Sinigoi, S., P. Comin-Chiaramonti, and A. A. Alberti, Phase relations in the partial melting of the Baldissero spinel lherzolite (Ivrea-Verbano zone, Western Alps, Italy), Contrib. Mineral. Petrol., 75, 111-121, 1980.

Sinigoi, S., P. Comin-Chiaramonti, G. Demarchi, and F. Siena, Differentiation of partial melts in the mantle: Evidence from the Balmuccia peridotite, Italy, Contrib. Mineral. Petrol., 82, 351-359, 1983.

Spear, F.S., An experimental study of hornblends stability and composition variability in amphibolite, Am. J. Sci., 281, 697-734, 1981.

Styles, P., and K. D. Gerdes, St. John's Island (Red Sea): A new geophysical model and its implications for the emplacement of ultramafic rocks in fracture zones and at continental margins, Earth Planet. Sci. Lett., 65, 353-368, 1983.

Toop, G. W., and C. H. Samis, Some new ionic concepts of silicate slags, Can. Metall. Q., 1, 129-152, 1962a.

Toop, G. W., and C. H. Samis, Activities of ions in silicate melts, Trans. Metall. Soc. AIME., 224, 878-887, 1962b.

Treuil, M., H. Jaffreric, N. Deschamps, C. Derre, F. Guichard, J. L. Joron, B. Pellettier, S. Novotny, and C. Courtois, Analyse des lanthanides, du hafnium, du scandium, du chrome, du manganese, du cobalt, du cuive et du zinc dans les mineraux et les roches par activation neutronique, J. Radioanal. Chem., 18, 155-165, 1973.

Varne, R., Hornblende lherzolite and the upper mantle, Contrib. Mineral. Petrol., 27 45-51, 1970.

Vielzeuf, D., and J. Kornprobst, Crustal splitting and the emplacement of Pyrenean lherzolites and granulites, Earth Planet. Sci. Lett., 67, 87-96, 1984.

Wass, S. Y., and N. W. Rogers, Mantle metasomatism-precursor to continental alkaline volcanism, Geochim. Cosmochimc. Acta, 44, 1811-1823, 1980.

Watson, E. B., Two-liquid partition coefficients: Experimental data and geochemical implications, Contrib. Mineral. Petrol., 56, 119-134, 1976.

Watson, E.B., Apatite and phosphorus in mantle source regions: An experimental study of apatite-melt equilibria at pressures to 25 kbar, Earth Planet. Sci. Lett., 51, 322-335, 1980.

Weale, K.E., Chemical Reactions at High Pressures, Barnes and Noble, New York, 1967.

Wells, P. R. A., Pyroxene thermometry in single and complex systems, Contrib. Mineral. Petrol., 62, 129-139, 1977.

Wendlandt, R. F., and W. J. Harrison, Rare earth partitioning between immiscible carbonate and silicate liquids and CO_2 vapor: Results and implications for the formation of light rare earth-enriched rocks, Contrib. Mineral. Petrol., 69, 409-419, 1979.

Wood, J. A., The Solar System , Prentice-Hall, Englewood Cliffs, N. J., 1979.

Yoder, H. S., and H. P. Eugster, Phlogopite synthesis and stability range, Geochim. Cosmochim. Acta, 6, 157-165, 1954.

Zielinski, R. A., and F.A. Frey, An experimental study of the partitioning of a rare earth element (Gd) in the system diopside-aqueous vapor, Geochim. Cosmochim. Acta, 38, 545-565, 1974.

E. Bonatti, Lamont-Doherty Geological Observatory of Columbia University, Palisades, NY 10964.

P. R. Hamlyn, Department of Geology, University of Melbourne, Melbourne, Australia.

G. Ottonello, Istituto di Geocronologia e Geochimica Isotopica del CNR, via Cardinale Maffi 36, 56100 Pisa, Italy.

(Received June 13,1985;
revised September 24,1985;
accepted September 24,1985)